A tuneable minimal cell membrane reveals that two lipid species suffice for life

Authors: Isaac Justice[a], Petra Kiesel[b], Nataliya Safronova[a], Alexander von Appen[b], and James P. Saenz[a, c]*

[a] Technische Universität Dresden, B CUBE Center for Molecular Bioengineering, 01307 Dresden, Germany

[b]Max Planck Institute of Molecular Cell Biology and Genetics, Pfotenhauerstrasse 107, 01307 Dresden

[c]Technische Universität Dresden, Faculty of Medicine, Dresden 01307, Germany

*corresponding author and lead contact: james.saenz@tu-dresden.de

Abstract

All cells are encapsulated by a lipid membrane which facilitates the interaction between life and its environment. How life exploits the diverse mixtures of lipids that dictate membrane property and function has been experimentally challenging to address. We introduce an approach to tune and minimize lipidomes in *Mycoplasma mycoides* and the Minimal Cell (JCVI-Syn3A) revealing that a 2-component lipidome can support life. Systematically reintroducing phospholipid features demonstrated that acyl chain diversity is more critical for growth than head group diversity. By tuning lipid chirality, we explored the lipid divide between Archaea and the rest of life, showing that ancestral lipidomes could have been heterochiral. Our approach offers a tunable minimal membrane system to explore the fundamental lipidomic requirements for life, thereby extending the concept of minimal life from the genome to the lipidome.

Introduction

Cell membranes are complex and responsive systems that serve to protect and mediate interactions of life with its environment. A large part of this molecular complexity is due to the diverse panel of lipids that make up the lipidome and which ultimately determine the form and function of the membrane. The complexity of cellular lipidomes can be staggering, from tens of unique structures in bacteria[1], to hundreds in eukaryotic organisms[2]. How life has evolved to utilize such complex mixtures of lipids to build cellular membranes remains an active area of exploration[1,3–6]. While synthetic membranes can be constructed using a single lipid species, the minimal number of lipid species required for a functional cell membrane remains undetermined. Identifying a minimal viable lipidome would provide a critical starting point for elucidating the combinations of lipid structures that are essential for membrane integrity and function, offering insights into the fundamental chemical and physical requirements of cellular life.

One approach to studying lipidome complexity is to experimentally manipulate lipidome composition and observe effects on cell fitness (e.g. growth). Bacterial model organisms have proven to be excellent systems for tuning lipidome composition by genetically disrupting lipid biosynthesis[7]. For example, early work with *Escherichia coli* mutants deficient in fatty acid synthesis explored the role of acyl chain unsaturation for cell growth[8], and a similar approach with *Bacillus subtilis* mutants explored the role of branched acyl chains[9]. More recent work, employing approaches to tune lipid unsaturation revealed the importance of homeoviscous adaptation for electron transport[10] and demonstrated how low membrane fluidity can induce phase separation, impaired membrane potential, cell growth and division[11]. However, for interpreting how lipidome composition and flexibility are affected by perturbed lipid synthesis, *E. coli*, like many bacteria, is complicated by the fact that it has multiple membranes (e.g. inner and outer). Changes in a single membrane are obfuscated by whole cell lipid extracts, and purifying specific membrane types is laborious, and can lead to substantial experimental error due to varying purity. Gram positive organisms such as *B. subtilis*, that have only a single membrane are better models in this regard[12,13]. However, traditional genetic approaches to tuning lipidome composition have so far not afforded complete control over both lipid class

53 composition, and phospholipid acyl chain composition. Thus, a cellular model system in which
54 lipidome complexity can be reduced in a systematic fashion has not yet been established.

55 *Mycoplasmas* are a genus of genomically simple bacterial pathogens possessing several
56 features that are promising as tunable living model membrane systems. *Mycoplasmas* have a
57 single plasma membrane, and lack a cell wall[14]. Therefore, their membrane composition and
58 biophysical properties can be examined *in situ* without the need for laborious membrane
59 isolation. Having evolved to a parasitic lifestyle, *Mycoplasmas* have lost many pathways for
60 biomolecular synthesis, including most of their lipid synthesis pathways, , relying instead on lipids
61 acquired from their hosts or from the growth media[14–18]. This affords the possibility to control
62 their lipidome composition by controlling what lipids are provided in the media. Further, because
63 of their relatively small genomes, the number of components involved in managing lipidome
64 composition and membrane adaptation is within reach of being completely characterized and
65 modeled[19]. Recently, a minimal cell, JCVI-Syn3.0, was engineered from *Mycoplasma mycoides*
66 *subsp. capri* strain GM12 by systematically removing genes from *M. mycoides* to achieve an
67 organism where every remaining gene is essential or quasi-essential[20]. However, this organism
68 exhibited pleomorphism and irregular cell division[21]. To restore normal cell division, a new strain,
69 JCVI-Syn3A was created with 19 additional genes not present in JCVI-Syn3.0. The addition of
70 these genes resulted in a regularly dividing quasi minimal cell which offers a platform to study
71 the role of lipids for the most fundamental requirements of life in a genomically minimized
72 system.

73 In this study, we establish an approach to modulate lipidome composition and reduce its
74 complexity in *M. mycoides* and JCVI-Syn3A. By tuning the lipid composition of the growth medium
75 and introducing diether phospholipids we introduce an approach to bypass cellular lipid
76 remodeling, achieving a lipidome with only two lipids. Using these lipidomically minimal living
77 membranes, we compare the relative importance of phospholipid head group vs. acyl chain
78 complexity. Additionally, we observed profound effects resulting from subtle changes in the lipid
79 chirality that distinguishes Archaea from the rest of life. By developing approaches to tune and
80 minimize mycoplasma lipidome composition, we hope to introduce a new tool for deciphering

81 the principles of living membranes and to introduce a new paradigm for understanding why life
82 has evolved to utilize so many lipids.
83

84 ## Results

85 ***Mycoplasmas as minimal model membrane systems***

86 *Mycoplasma mycoides* is a pathogen of mammals that has historically been used as a
87 simple model membrane system. There are a number of reasons why *M. mycoides* makes a good
88 model membrane system. First, its small genome (~1,100,000 bp) limits the complexity of its
89 genetic regulation, and has allowed researchers to fully sequence and annotate the genome
90 (although a number of genes still have unknown or only putative functional assignments)[22].
91 Second, as a pathogen, the primary source of lipids for *M. mycoides* is through environmental
92 uptake from the host rather than synthesis[14–16,23]. In a laboratory setting using growth medium
93 as the lipid source, this feature provides the experimenter with direct control over the lipid
94 components available for synthesizing and maintaining the membrane; by adding or removing
95 specific lipids from the growth medium of *M. mycoides*, the composition of the membrane can
96 be altered. Third, *M. mycoides* has a single plasma membrane and no cell wall or organelles,
97 making it easy to interrogate the membrane and ensuring that membrane targeting probes in *M.*
98 *mycoides* are acting on the membrane and not another structure[14]. Fourth, and perhaps most
99 importantly for this research, *M. mycoides* is unable to synthesize or alter fatty acid
100 composition[14–17]. This means that, while it can alter the acyl chain composition of its membrane
101 lipids, it is limited in its ability to do so by the pool of fatty acids it has access to. These factors
102 combine to make *M. mycoides* one of the model systems in which membrane remodeling is both
103 the simplest and most controllable, and as such it is an excellent model system to study
104 membrane remodeling in living organisms[24].
105

106 In *M. mycoides* membranes phospholipids, sterols, and free fatty acids are taken up from
107 the environment and either incorporated into the membrane or taken up into the cytoplasm (Fig.
108 1; 1)[14,25–27]. *M. mycoides* can cleave acyl chains from exogenous phospholipids (Fig. 1; 2)[28–30].
109 When a pool of free fatty acids is present, *M. mycoides* can use those fatty acids to modify the

110 acyl chain composition of phospholipids taken up from the media, or can synthesize the
111 phosphotidylglycerol (PG) class of lipids which can in turn be modified and used to synthesize
112 cardiolipin (CL) (Fig. 1; 3, 4, 5)[14,27,28,31–34]. These newly synthesized or modified lipids can be
113 broken down to replenish the fatty acid pool, or reinserted into the membrane (Fig. 1; 6, 7)[32].
114 With the exception of the modification of PG headgroups to make cardiolipin, all lipid remodeling
115 in *M. mycoides* is acyl chain remodeling–that is, it relies on having access to a pool of free fatty
116 acids to modify the existing acyl chain composition of phospholipids or synthesize *de novo*
117 PGs[14,15]. Cholesterol is essential for growth of *M. mycoides* (Fig. 1; 8)[26,35,36]. For the first time, we
118 report the feeding of *M. mycoides* on a defined lipid diet which contains no exogenous source of
119 free fatty acids. When fed such a diet, *M. mycoides* is forced to rely completely on acyl chain
120 scavenging from exogenous phospholipids as its only source of acyl chains for which to remodel
121 its membrane lipidome.
122
123 The diverse lipid structures that *M. mycoides* can take up or synthesize ultimately
124 determine the physical properties of their cell membranes[37,38]. Phospholipid acyl chains can vary
125 in terms of their length and degree of unsaturation, both influencing physical parameters such
126 as membrane fluidity, thickness, and permeability. Phospholipid headgroups such as PG and
127 cardiolipin introduce a negative surface charge to the membrane, which can influence their
128 interaction with peripheral membrane proteins. Conversely, PC is zwitterionic and introduces a
129 neutral charge to the membrane surface. The geometric shape of phospholipids is also important,
130 and determines whether a lipid spontaneously aggregates to form a bilayer or non-bilayer
131 structure. For example, cardiolipin has four acyl chains and a relatively small headgroup giving it
132 a conical profile. Cells have been shown to tune the abundance of such conical lipids to modulate
133 the curvature and bending rigidity of their membranes[39]. Sterols, which also do not form bilayers
134 by themselves, play an important biophysical role in the membrane, including in modulating
135 membrane fluidity, stability, facilitating liquid-liquid phase separation, and membrane
136 asymmetry[40,41]. By limiting the diversity of lipids that can be taken up or synthesized, we aimed
137 to identify a minimal viable lipidome that can be used as an experimental platform in which lipid
138 diversity can be systematically tuned in a living membrane.

139 ***Minimizing the lipidome***

140 Our first goal was to determine the minimal lipidome that can support growth of *M.*
141 *mycoides*. Sterols, preferably cholesterol, are required for growth, and must be included in any
142 lipid diet. *M. mycoides* can synthesize several phospholipids (e.g. PG and cardiolipin; Full lipid
143 names and abbreviations can be found in Table 1) when provided free fatty acids[14,27]. For
144 example, when grown on a lipid diet consisting of cholesterol, and two fatty acids (palmitate -
145 C16:0 and oleate - C18:1), the lipidome of *M. mycoides* contains primarily cholesterol, PG,
146 cardiolipin and small amounts of diacylglycerol (DAG) and phosphatidic acid (PA), both precursors
147 of PG synthesis (Fig 2b, Supplementary Table S3). Therefore, to minimize the phospholipid
148 diversity, we removed free fatty acids from the lipid diet and instead provided a single
149 phospholipid, 16:0/18:1 phosphatidylcholine (POPC), along with cholesterol, yielding a minimal
150 2-component lipid diet. When transferred from growth medium containing fetal bovine serum
151 (FBS, a complex undefined lipid source), to the two-component lipid diet, cells initially grew
152 poorly and tended to aggregate in clumps (not shown). Thin layer chromatography (TLC) of cell
153 lipid extracts showed that, initially, PG and cardiolipin (both internally synthesized lipids)
154 disappeared, and only traces of sphingomyelin (SM) remained, presumably carry over from
155 growth on FBS (Fig. 2a; full TLCs are shown in Supplementary Fig. S2). After adaptation (> 3
156 passages in batch culture), SM was no longer visible, however, phosphatidylglycerol (PG) and
157 cardiolipin reappeared along with lyso-PC (a PC lipid with one of its acyl chains removed, which
158 appears below the SM band). Since *M. mycoides* cannot synthesize phospholipids in the absence
159 of fatty acids, these observations indicate that acyl chains were being scavenged from POPC for
160 the synthesis of PG and cardiolipin, presumably as a result of lipase activity (Fig. 2a). A systematic
161 analysis of PG and cardiolipin production on minimal lipid diets composed of varying
162 phospholipid species demonstrated that *M. mycoides* is capable of scavenging acyl chains from a
163 broad range of phospholipid headgroups (Fig. S1, Table S2), demonstrating a robust capacity for
164 *M. mycoides* to procure acyl chains for internal PG and cardiolipin synthesis from nearly any
165 phospholipid source.

166 The capacity for *M. mycoides* to scavenge acyl chains from exogenous phospholipids
167 provided a hurdle to our goal of minimizing the lipidome. Shotgun mass spectrometry of cells
168 grown on the minimal 2-component lipid diet revealed 31 lipid species generated from the
169 remodeling of POPC (with 18 lipid species comprising 99% of the lipidome), and presence of
170 phospholipids including PG, cardiolipin, with small amounts of the PG precursors PA and DAG
171 (Fig. 2c, Table S3). Since the source of acyl chains for internal phospholipid synthesis presumably
172 came from exogenous POPC, we reasoned that internal lipid synthesis could be eliminated by
173 blocking acyl chain scavenging. To do this, we replaced POPC with an analogous lipid containing
174 ether-linked 16:0 and 18:1 hydrocarbon chains, which are inert to lipase activity[42,43]. Following
175 the transfer of cells from FBS or minimal POPC-cholesterol diet to a minimal Diether PC-diet, TLC
176 analysis of lipid extracts over several passages showed the disappearance of cardiolipin and PG,
177 and presence of only two bands corresponding to cholesterol and Diether PC (D.PC; Fig. 2a).
178 Shotgun lipidomic analysis demonstrated that cholesterol and D.PC accounted for 99.9 mol% of
179 the detected lipids (Fig. 2d) (the remaining very low abundance lipids are derived from impurities
180 in the media, in particular from yeast extract, Table S3). Thus, by introducing an enzymatically
181 inert phospholipid, D.PC, to the minimal lipid diet, we could achieve a minimal lipidome
182 composed predominantly of only two lipid species, cholesterol and D.PC.

183 ***Tuning lipidome composition***

184 Minimizing the lipidome of *M. mycoides* to two lipids resulted in a two-fold decrease in
185 growth rates (Figure. 3e, D.PC condition compared to POPC condition). We next asked which
186 components of the lipidome most effect growth. By feeding cells with D.PC, we had reduced
187 lipidome composition in several ways. First, we eliminated the presence of internally synthesized
188 phospholipids such as PG and cardiolipin. Therefore, minimizing the diversity of phospholipid
189 headgroups could have contributed to impaired growth. Second, we eliminated phospholipid
190 hydrocarbon chain diversity by limiting the cell to one configuration (16:0/18:1). Thus, it is also
191 possible that restricting the diversity of phospholipid hydrocarbon chain configurations could
192 have impaired growth.

193 To investigate the importance of head group diversity and structure on determining
194 growth rate we provided cells with lipid diets containing Diether PG (D.PG) and a mixture of D.PG
195 with D.PC. When lipid extracts of cells grown on D.PG were analyzed by TLC, we observed bands
196 corresponding to both PG and cardiolipin, indicating that cardiolipin synthesis can proceed from
197 D.PG (Fig. 3a). When grown on D.PG and D.PC, TLC analysis showed three bands corresponding
198 to PC, PG, and cardiolipin (Fig. 3b). Thus, cells grown on D.PC generate lipidomes with one
199 phospholipid headgroup, those on D.PG produce lipidomes with two headgroups, and cells
200 grown on both D.PG and D.PC yield lipidomes with three headgroups. Specifically, D.PC cells have
201 only a neutral, bilayer-forming phospholipid, while D.PG cells contain negatively charged
202 phospholipids, including both bilayer-forming (PG) and non-bilayer-forming (cardiolipin) types.
203 In D.PC + D.PG cells, both neutral and negatively charged phospholipids, as well as bilayer- and
204 non-bilayer-forming types, are present. Surprisingly, despite this increased lipidome complexity,
205 the introduction of negatively charged (PG) or conical non-bilayer-forming (cardiolipin)
206 phospholipids did not improve growth rates compared to D.PC cells (Fig. 3e; full growth curves
207 are shown in Supplementary Fig. S4a). To put these values in context, the growth rates we
208 estimate from all of the defined diets considered in this study are more than 10-fold lower than
209 for cells grown on a complex FBS lipid diet, highlighting the effect of reducing lipid diet complexity
210 on growth[44]. Indeed, growth rates for both D.PG and D.PG + D.PC diets were slightly lower than
211 for D.PC alone (Fig. 3e). It is possible that this result is due to the fact that the synthesis of
212 cardiolipin from D.PG results in a single cardiolipin species with hydrocarbon chains of fixed
213 length and saturation, meaning that the *M. mycoides* cannot remodel cardiolipin to optimize acyl
214 chain structure[6]. Further, growth of cells on POPC prior to adaptation and ability to synthesize
215 PG and cardiolipin, show only slightly higher growth rates than D.PC diets, indicating that reduced
216 growth is not solely due to the introduction of diether phospholipids. Phospholipid headgroup
217 diversity alone, therefore, is not sufficient to rescue growth.

218 To understand the impact of phospholipid acyl chain diversity on cell growth, we grew
219 cells on a diet of cholesterol and two fatty acids (palmitate and oleate), designated as '2FA'. On
220 this diet, the phospholipidome is predominantly composed of PG and cardiolipin (Fig. 2b),
221 allowing for the synthesis of phospholipids with various acyl chain configurations (e.g., 16:0/18:1

222 POPG, 16:0/16:0 DPPG, 18:1/18:1 DOPG for PG, and different permutations of PGs as substrates
223 for cardiolipin synthesis). Although DAG and PA are present in low abundances (1.8 mol%, and
224 0.3 mol%, respectively, Supplemental Table S3), they are also both conical-shaped lipids, similar
225 to cardiolipin. In that respect, their contribution to the membrane's physical properties is
226 relatively small and does not introduce significant differences compared to what is already
227 provided by the far more abundant cardiolipin. Therefore, while the 2FA diet exhibits comparable
228 headgroup diversity to cells grown on D.PG, they exhibit greater acyl chain diversity. Growth rates
229 on the 2FA diet were more than double those on D.PG and approached the growth rates of cells
230 adapted to POPC (Fig. 3e). This suggests that for a lipidome with predominately two phospholipid
231 headgroups, increased acyl chain diversity can rescue growth. An important consideration in
232 comparing cells grown on the 2FA diet versus the D.PC + D.PG diet is that phospholipids with
233 diether-linked acyl chains are not natural for this organism and could introduce a growth deficit.
234 However, the similar growth rates observed in cells grown on POPC prior to adaptation, which
235 could not yet synthesize PG and cardiolipin, compared to D.PC diets, suggest that reduced growth
236 is not primarily due to the introduction of diether phospholipids. Acknowledging that differences
237 in natural ester linkages and unnatural ether linkages, and the presence of DAG and PA—albeit
238 in low abundance—may also influence the observed growth rates, these observations suggest
239 that acyl chain complexity is an important factor in rescuing growth.

240 Finally, we asked whether growth could also be rescued by providing the full suite of 31 lipids in
241 cells adapted to growth on POPC. It is possible, for example, that growth is impaired by the
242 disruption of internal phospholipid synthesis or remodeling pathways due to coupling of lipid
243 synthesis with cellular growth. To test this, we took advantage of the fact that when cells grown
244 on the minimal lipid diet are switched to a diet containing ester phospholipids (e.g. POPC +
245 cholesterol) there is a period of adaptation similar to that seen in Fig. 2a. After the first passage,
246 before adaptation, the cells do not yet undergo detectable acyl chain scavenging, and the
247 membrane composition remains predominantly composed of the two lipids POPC and
248 cholesterol (Fig. 3d). This delayed adaptation to acyl chain scavenging allows us a brief window
249 to study simplified membranes composed of lipids *M. mycoides* could normally scavenge acyl
250 chains from. The simplified membranes only persist until *M. mycoides* is adapted to the new diet

251 after several passages. We thus transferred cells grown on the minimal diet (D.PC + cholesterol)
252 to a lipid diet derived from lipid extracts of cells adapted to growth on POPC (Fig. 3e), and
253 measured growth in the first passage, before cells adapted to scavenge acyl chains from the
254 dietary phospholipids. Growth rates on this transplanted lipidome diet resulted in a nearly
255 complete rescue to levels observed in POPC cells after adaptation (Fig. 3e). These results indicate
256 that internal phospholipid synthesis and remodeling are not required for optimal growth, and
257 demonstrates a proof-of-principle that functional lipidomes can be engineered and transplanted
258 to living membranes to support growth.

259 ***Minimizing the lipidome of the Minimal Cell***

260 JCVI-Syn3A is a synthetic cell created by the J. Craig Venter Institute (JCVI) by removing
261 every non-essential gene from *M. Mycoides*[20]. To do this, Hutchison et al. conceptually divided
262 the genome of *M. mycoides* into 8 segments and systematically went through each, removing
263 genes to see which were essential or non-essential. As such, JCVI-Syn3A is genomically an even
264 simpler model system than *M. mycoides*, while still possessing all of the previously described
265 characteristics of *M. mycoides* that make it a valuable model membrane system[45]. In this study,
266 we used a strain that expresses an additional gene for the fluorescent mCherry protein, to create
267 JCVI-Syn3A-*mCherry*[21,46], which for simplicity we subsequently refer to as JCVI-Syn3A. JCVI-Syn3A
268 provides a good comparison organism to *M. mycoides*, and an experimental platform to examine
269 the role of lipidome composition in supporting the minimal requirements for life. We therefore
270 asked whether the JCVI-Syn3A lipidome could also be minimized.

271 Since JCVI-Syn3A has a truncated set of genes compared to *M. mycoides*, we first tested
272 whether they retained the capacity to scavenge acyl chains from exogenous phospholipids for
273 the internal synthesis of PG and cardiolipin. Unexpectedly we observed that, like *M. mycoides*,
274 JCVI-Syn3A could still synthesize PG and cardiolipin when fed with a minimal 2-component diet
275 of cholesterol and POPC, as well as with a range of other phospholipid head groups
276 (Supplementary Table S2). This suggests that an undiscovered lipase remains in the JCVI-Syn3A
277 genome. The presence of such lipase activity in a genomically minimal cell could mean that it is
278 essential. Alternatively, it could also indicate that, while not essential itself, it is a secondary
279 "moonlighting" activity of an enzyme with an essential activity[47]. This implies that with the

280 appropriate complement of lipids, the genome could be further minimized by eliminating genes
281 involved in lipid remodeling activities.

282 Next, we assayed growth of JCVI-Syn3A on a 2-component lipid diet of cholesterol + D.PC.
283 Growth for JCVI-Syn3A and *M. mycoides* on the D.PC + Cholesterol diet are commensurate, but
284 on the POPC + Cholesterol diet *M. mycoides* has significantly improved growth (Fig. 4a). By
285 comparison, cells grown on FBS, a complex lipid diet, exhibit ~ 10-fold higher growth rates[44].
286 Although growth is exceptionally slow, the culture can be continuously passaged in batch, and
287 samples taken 24 hours post-inoculation consistently yield colony-forming units, confirming the
288 viability of the cells (Supplementary Fig S5). Shotgun lipidomic analysis confirmed that JCVI-Syn3A
289 cells grown on a 2-component D.PC + cholesterol diet yielded a lipidome with over 99 mol%
290 composed of only two lipid species (Fig. 4b, Table S3). As such, this work has developed the
291 simplest known living membrane in one of the simplest known living organisms.

292 Previous studies reported that genome minimization in JCVI-Syn3.0 caused pleomorphic
293 traits and abnormalities in cell division, which were rescued by reintroducing 19 genes, resulting
294 in the creation of JCVI-Syn3A[21]. Given that a reduced lipidome could also impair cellular functions,
295 we investigated whether lipidome minimization might lead to abnormal cell morphologies in
296 JCVI-Syn3A. Transmission electron microscopy (TEM) images of JCVI-Syn3A grown on three
297 different lipid diets—fetal bovine serum (FBS), POPC + cholesterol, and D.PC + cholesterol—
298 revealed mostly typical ovoid cells (Fig. 4c, TEM overview images provided in Supp. Fig. 6a-g).
299 However, two distinct morphological features were observed in subpopulations of cells: internal
300 membrane-encapsulated vesicles and tube-like membranous structures connecting cells.

301 The tubules observed in fewer than 20% of cells, were less frequent in cells grown on
302 POPC or D.PC compared to those grown on FBS. These structures are reminiscent of those seen
303 in wall-less L-form bacteria, where they are hypothesized to function as an FtsZ-independent
304 mechanism, possibly representing a primitive form of cell division[48]. Further investigation is
305 required to determine if the tubules observed in JCVI-Syn3A are functional or represent
306 incomplete cell division. Notably, their higher prevalence in FBS-grown cells suggests that they
307 are not directly related to lipidome minimization.

308 In contrast, the frequency of cells with membrane invaginations increased more than two-
309 fold from ~15% in FBS-grown cells to nearly 40% in those grown on D.PC. In some instances, these
310 invaginations appeared as distinct membrane-encapsulated vesicles within the cell, separate
311 from the cell surface membrane. To confirm the presence of these internalized membrane
312 vesicles, we used cryogenic electron microscopy (cryoEM) to construct whole-cell tomograms.
313 Tomograms of JCVI-Syn3A from all three diets confirmed the presence of internal membrane-
314 encapsulated vesicles (Fig. 4d, Supp. Fig. S6h-i). The lower electron density within these vesicles
315 (pixel brightness), compared to the cytoplasm, indicates they result from membrane
316 invagination, encapsulating extracellular fluid.
317 Interestingly, cells with reduced lipidomes were larger on average compared to those
318 grown on FBS (~0.75 um vs. 0.3 um diameter respectively), as estimated semi-quantitatively from
319 TEM images (Supplementary Fig. S6j). Cells with internal vesicles were particularly enlarged
320 across all conditions (up to 1.5 um average diameter). These results suggest that lipidome
321 minimization leads to larger cell sizes and a higher frequency of membrane invaginations,
322 indicative of impaired regulation of cell size and shape. The increased frequency of membrane
323 invaginations could result from non-optimal membrane bending rigidity or intrinsic curvature
324 from the loss of cardiolipin, and acyl chain diversity. Nonetheless, the fact that around half of the
325 observed cells maintained normal morphology shows that even with just two lipid species, JCVI-
326 Syn3A is capable of preserving typical cell morphology.
327
328 ***Tuning lipid chirality***
329 Having explored the minimal requirements for lipidome complexity in *M. mycoides* and
330 JCVI-Syn3A, we next sought to leverage these model systems to probe another fundamental
331 aspect of lipid biology: chirality. Glycerolipids (including phospholipids) have a chiral center in the
332 glycerol backbone leading to enantiomeric lipids that are mirror images of each other (Fig. 5a).
333 In bacteria and eukaryotes, glycerolipids are synthesized with acyl chains at the sn-1 and sn-2
334 positions, and the phosphate head group at the sn-3 position (Fig. 5a: G3P enantiomer).
335 Conversely, archaea synthesize glycerolipids with the phosphate at the sn-1 position and the acyl
336 chains at the sn-2 and sn-3 positions (G1P enantiomer)[49,50]. Known as the 'Lipid Divide', this

337 difference in stereochemistry between lipids of archaea and the rest of life has long stood as an
338 unexplained enigma[51–54]. Did a last common ancestor have membranes with both enantiomers?
339 What are the consequences of having a racemic mixture of phospholipids in a living membrane?
340 To date, no naturally occurring organism has been found that has comparable amounts of both
341 enantiomers in its membrane. Furthermore, experimentally modulating phospholipid chirality in
342 the lipidome through genetic approaches presents significant challenges, as shown by the work
343 of Caforio et al[54]. However, the ability of mycoplasma to uptake exogenous lipids makes them an
344 exceptionally well-suited model for unraveling this elusive problem in membrane biology.

345 To establish whether *M. mycoides* and JCVI-Syn3A can grow on a G1P phospholipid
346 enantiomer, we prepared a lipid diet consisting of cholesterol and enantiomeric POPC (entPOPC),
347 as well as a racemic mixture of cholesterol and POPC:entPOPC (1:1 mol%). We compared the two
348 diets containing entPOPC against growth on cholesterol + POPC (Fig. 5b, 5c). Growth rates
349 derived from Phenol Red absorbance of both organisms show that the introduction of entPOPC
350 to the lipid diet results in impaired growth, with the racemic diet yielding the most pronounced
351 decrease in growth rate. We also evaluated growth by measuring optical density, as a proxy for
352 cell density (Supplementary Figure S7), which confirmed a reduction in growth with the
353 introduction of entPOPC. However, in contrast, growth was similar for the entPOPC and racemic
354 lipid diets. This difference likely reflects the fact that Phenol Red growth rate estimates reflect
355 metabolic activity, which is not necessarily coupled with the production of cell biomass measured
356 by optical density. Thus, we demonstrate that cells are viable when fed enantiomeric
357 phospholipids.

358 We next asked how the introduction of entPOPC affected the mechanical robustness and
359 permeability of the membrane. To assay membrane robustness, we measured sensitivity of cells
360 to hypoosmotic shock, by determining what fraction of cells are lysed following a shock. Since *M.*
361 *mycoides* and JCVI-Syn3A lack a cell wall or cytoskeleton, cell lysis during rapid hypoosmotic shock
362 is indicative of membrane rupture strength. Furthermore, mechanosensitive ion channels which
363 can protect cells from hypoosmotic shock have, to the best of our knowledge, not been reported
364 in either organism, or annotated in the genomes, and are not present in all *Mycoplasmas*[47,55].
365 Therefore, it is reasonable to cautiously interpret the susceptibility to lysis from hypoosmotic

366 shock as indicative of membrane stability. However, we cannot rule out the possibility that there
367 are undiscovered mechanosensitive channels, and this would suggest that mechanosensitive
368 gating is sensitive to lipid chirality. Hypoosmotic sensitivity increased significantly for cells grown
369 on entPOPC diets, indicating that the enantiomeric lipids affect the mechanical robustness of the
370 membrane and, consequently, the whole cell (Fig. 5b, c). To assay permeability, we measured
371 the rate of permeation of fluorescein diacetate (FDA), a non-chiral molecule, across the cell
372 membrane[56,57]. Membrane permeability, as measured by the permeability coefficient of FDA
373 increased significantly upon the introduction of enantiomeric lipids, but was the highest for both
374 *M. mycoides* and JCVI-Syn3A for the racemic lipid diet (Fig. 5b, c). When plotted against growth
375 rate, there is an apparent correlation of lower growth with higher permeability (Fig 5d, e),
376 possibly indicating membrane leakiness as one of the factors underlying impaired growth. The
377 permeability coefficients were similar to those previously reported in mammalian cells[57].
378 Increased permeability and reduced membrane robustness could be due either to
379 changes in the property of the lipid bilayer, or through changes in lipid-protein interactions.
380 Previous work on PC enantiomers in model membranes revealed that modest changes in
381 permeability to calcein occur in membranes composed of both enantiomers, in particular
382 scalemic (not 1:1) mixtures. However, such small changes would not account for the large change
383 in permeability we observe. To determine if introducing enantiomeric POPC affected membrane
384 bilayer robustness or permeability we reconstituted cellular lipid extracts from *M. mycoides* into
385 liposomes and evaluated C-Laurdan fluorescence (Fig. 6). The C-Laurdan General Polarization
386 index (GP) reports bilayer hydration, which is closely coupled with permeability and mechanical
387 robustness of the membrane[58,59]. Surprisingly, GP values did not vary significantly across all three
388 POPC diets, indicating that the lipid bilayer itself was not disrupted by changes in chirality, and
389 implicating an effect on lipid-protein interactions. Indeed, several studies have demonstrated an
390 effect of varying lipid chirality on lipid-peptide interactions, and the permeability of membranes
391 to chiral amino acids[60,61]. Thus, disrupted lipid-protein interactions are the most likely basis for
392 the observed phenotypes, setting the stage for future work employing *M. mycoides* and JCVI-
393 Syn3A as model systems to explore the significance of lipid chirality on lipid-protein interactions
394 in a living membrane.

395

396 ## Discussion

397 In this study, we introduce *M. mycoides* and the Minimal Cell JCVI-Syn3A as simple model
398 organisms with tunable lipidomes for studying the role of lipid complexity. By choosing a model
399 membrane system incapable of synthesizing or modifying fatty acids, and developing a set of
400 defined lipid diets for that system, we have demonstrated the creation of a platform in which the
401 lipidome can be tuned in terms of phospholipid head group, acyl chain composition or lipid
402 chirality. Using this platform, we created the simplest living membrane, and one incapable of
403 undergoing acyl chain remodeling. These tunable living membranes allowed us to quantitatively
404 examine the contribution of lipidomic features to the fitness of a minimal living system.

405 ***Lipid scavenging***

406 Our observations broadly demonstrate how lipidome composition is crucial even for
407 relatively simple microorganisms. This is anecdotally illustrated by the capacity we observe for
408 mycoplasma to produce a complex lipidome from a single exogenous phospholipid, which is an
409 impressive evolutionary adaptation to their pathogenic lifestyle. Indeed, this acyl chain
410 scavenging activity, which confounded our initial attempt to simplify the lipidome, suggests a
411 potential target for treating mycoplasma infection. Although mycoplasma can survive in pure
412 culture with a reduced lipidome, they may fare much worse in the context of a host immune
413 system. Furthermore, the ability for the Minimal Cell to grow with a lipidome of two lipids implies
414 the possibility for further minimization of the genome, through the deletion of pathways involved
415 in the scavenging of phospholipid acyl chains and the internal synthesis of phospholipids.

416 ***Minimal lipidomes***

417 A long-standing challenge in membrane biology has been to understand why life has
418 evolved such complex lipidomes and to identify the essential features of lipidomes required for
419 optimal membrane function and cellular fitness. The simplest lipidome so far reported was from
420 a Gram-negative bacterium, composed of 27 lipid species, excluding outer membrane
421 lipopolysaccharides that were not analyzed[1]. By reducing the lipidome of M. mycoides and JCVI-
422 Syn3A down to two lipids, we show that a complex lipidome is not essential for life, but that two
423 lipids are far from optimal.

424 Through systematic reintroduction of lipidomic features into cells with a minimal
425 lipidome, we demonstrated that phospholipid headgroup diversity alone does not significantly
426 rescue growth. Consistently, minimizing headgroup diversity in *B. subtilis* has little effect on
427 growth[13]. Similarly, E. coli mutants lacking phosphatidylglycerol (PG) and cardiolipin can be viable
428 and often do not exhibit significant growth deficiencies[7,62]. It was perhaps most surprising that
429 M. mycoides grew comparably well in the absence of zwitterionic lipids (PC), which are essential
430 for *E. coli* to support proper membrane insertion and activity of membrane proteins[63]. These
431 observations emphasize the limited impact of headgroup diversity, at least in simple bacterial
432 organisms, in the absence of other critical lipid features.
433 Restoring acyl chain diversity, in contrast, did enhance growth rates. This finding is
434 consistent with recent work showing the importance of acyl chain unsaturation in various cellular
435 processes, including the assembly and function of the nuclear pore complex in eukaryotes[64] and
436 in neuronal membranes[65]. The enhanced growth observed when acyl chain diversity was restored
437 in *M. mycoides* suggests that while headgroup diversity alone is insufficient, it may contribute to
438 improved cellular fitness when coupled with the appropriate acyl chain composition. For
439 example, the introduction of cardiolipin or PG could potentially improve growth, but only if these
440 lipids are present with the correct acyl chain configurations that support optimal membrane
441 properties and lipid-protein interactions. The approach to tuning the lipidome that we introduce
442 here provides a platform to explore the synergistic effects of specific acyl chain-headgroup
443 combinations, to unravel how these lipidomic features can be optimized for membrane function
444 and cellular fitness in minimal systems.
445 By applying a targeted chemical approach to reduce the lipidome of JCVI-Syn3A,
446 we demonstrated the feasibility of further simplifying the molecular composition of a
447 genomically minimized organism. The observation that a minimal cell membrane can function
448 with only cholesterol and one species of PC demonstrates that the fundamental requirements
449 for life can be achieved with a remarkably simple lipid composition. For synthetic biology, this
450 insight simplifies the challenge of designing synthetic cells, revealing the potential to create
451 functional living membranes with minimal components. This work lays a foundation for future

452 efforts to understand how minimal lipidomes can be optimized in synthetic and engineered
453 biological systems

454 One limitation of this work is that the growth medium is not defined, and there is a very
455 small contribution of lipids from components of the growth medium, such as the yeast extract.
456 Thus, while the majority (>99%) of the minimal lipidome is composed of 2 lipids, there is a fraction
457 of a percent of very low abundance lipids derived from the media and it is possible, but unlikely,
458 that these trace lipids play a significant role. In this regard, development of a defined growth
459 medium will be essential in the continued development of mycoplasmas as minimal model
460 membrane systems[33]. Another factor limiting the minimization of the lipidome to one lipid is that
461 cholesterol (or an analogue) is required for growth, but also cannot form a bilayer alone. So, it is
462 possible that even one bilayer forming lipid could support life in a cell that has not evolved to
463 require sterols. It is also, however, possible that having a membrane reinforcing sterol or sterol
464 analogue is critical for building a stable cell membrane with only one phospholipid. A
465 mycoplasma-like organism such as *Mesoplasma* that does not require sterols for growth would
466 provide a means to test this hypothesis[66–68]. Nonetheless, a JCVI-Syn3A membrane with two lipids
467 comprising over 99% of the lipidome is currently the simplest living membrane that has been
468 reported.

469 ***Lipid chirality and the lipid divide***

470 The lipid divide represents another major problem in membrane biology. Homochirality
471 is a fundamental feature of biomolecular chemistry. Biomolecules exhibit enantioselectivity for
472 chirally compatible interaction partners. Consequently, life has evolved to rely on homochiral
473 molecules (e.g. L-amino acids and nucleic acids). An interesting twist is in the divide between the
474 chirality of phospholipids made by Archaea and the rest of life[69]. The divide raises questions
475 about whether the last universal common ancestor (LUCA) possessed a heterochiral lipidome, or
476 whether the divide happened after the divergence of Bacteria and Archaea[70,71]. Further, current
477 theories that eukaryotes emerged from an Archaeal ancestor[72], create a conundrum in explaining
478 why Eukaryotes don′t have Archaeal lipid enantiomers, and whether a gradual transition
479 involving heterochiral lipidomes could have occurred. At the crux of these conundrums is
480 whether heterochiral lipidomes can support stable membranes and optimal cellular fitness.

481 We took advantage of the tuneability of *M. mycoides* and JCVI-Syn3A lipidomes to
482 observe how heterochiral lipidomes influence the membrane and cellular growth. Previous work
483 in living systems has achieved lipidomes with a mixture of structurally diverse bacterial and
484 archaeal lipids that differed not only by chirality, but also in a variety of other ways[54]. A unique
485 feature of this study is that we were able to introduce two enantiomers of a single lipid structure
486 (POPC) into a living membrane. Our results demonstrate that a heterochiral lipidome results in a
487 leakier membrane and impaired cellular robustness and growth. In contrast, previous work in *E.*
488 *coli* indicated that heterochiral lipidomes did not affect growth[54]. *E. coli* has an outer membrane
489 and cell wall that might compensate for lack of stability caused by heterochirality. The lipids in
490 the *E. coli* study were not stereoisomers, but rather entirely different lipid structures (ether vs.
491 ester acyl chain linkages, isoprenoid tails vs. fatty acid tails). It is possible that these structural
492 differences somehow obscured the destabilizing effects of heterochirality. Ultimately, the basis
493 for these diverging observations will provide insight into the biological significance of lipid
494 chirality. Nonetheless, our work shows that in a minimal organism with a single membrane,
495 heterochiral lipidomes can support growth, but lead to impaired robustness and fitness.
496 Interestingly, this suggests that LUCA could have existed before the evolution of homochiral
497 cellular membranes. This possibility would eliminate the need to view the lipid divide between
498 bacteria and archaea as resulting from independent evolutionary events. Instead, it suggests the
499 ancestral lipidome could have been heterochiral, consistent with a simpler path for the evolution
500 of modern membranes. Additionally, the reduced fitness and increased membrane permeability
501 resulting from heterochiral lipidomes suggests selective pressure against such membranes in
502 ancestral organisms, favoring the evolution of the homochiral membranes characteristic of
503 modern life.

504 The changes in membrane robustness and permeability that we observed do not seem to
505 be explained by changes in lipid order of pure lipid vesicles reconstituted from cell lipid extracts
506 of homo- and heterochiral lipidomes. This implies that lipid-protein interactions are
507 enantioselective and may be affected by lipid chirality in ways that impair membrane robustness
508 and function. Numerous *in vitro* studies have demonstrated the effect of lipid chirality on lipid-
509 protein interactions, consistent with the possibility that the phenotypes we observed are rooted

510 in perturbed lipid-protein interactions. Looking forward, *M. mycoides* and JCVI-Syn3A will be
511 excellent model system to explore the functional consequences of lipid chirality on lipid-protein
512 interactions.

513 ***Outlook***

514 Our approach to employ *M. mycoides* and JCVI-Syn3A as minimal living model membrane
515 systems paves a new path towards unraveling the role of lipidome diversity and complexity. Our
516 observations reveal that life does not require complex lipidomes. However, minimization comes
517 with clear trade-offs in cellular fitness. We further demonstrate the capacity of these model
518 systems to serve as chassis for exploring fundamental questions in membrane biology. The ability
519 of this system as a testing platform for lipid diets with a variety of features (including class and
520 acyl chain composition) makes it a useful and simple *in vivo* model for design-test-build
521 applications of membrane composition experiments. Furthermore, we demonstrated the ability
522 to force *M. mycoides* and JCVI-Syn3A to take up and incorporate enantiomeric lipids in their
523 membranes, the first time this has been shown in eukaryotic or prokaryotic organisms, and an
524 exciting first step to allow us to probe questions about the lipid divide and the role of chirality in
525 membrane stability and cell fitness. Overall, we have demonstrated the creation of a simple,
526 tunable, living, model membrane system that can be used as a novel platform for probing the
527 design principles of living membranes.

528

529 **Acknowledgements**

530 The authors wish to thank the Saenz lab; Lisa Junghans, Ha Ngoc Anh Nguyen, and Tomasz
531 Czerniak for discussions and feedback through the process, and for help with experimental
532 designs; the JCVI, and specifically John Glass and Kim Wise, for providing *M. mycoides* and JCVI-
533 Syn3A and for further feedback, including manuscript comments; Helena Jambor for assisting
534 with figure design; and Jennifer Katz-Brandoli for assisting with robot runs and figure
535 construction. We would like to thank Telesis Bio, Inc. for allowing us to use JCVI-syn3A and
536 Lipotype GmbH for lipidomic analyses. We would like to thank the Electron Microscopy Facility
537 of the MPI-CBG for their support. We additionally wish to thank Michaela Wilsch-Bräuninger from
538 the MPI-CBG for insights regarding EM images, Mareike Jordan from the Von Appen Lab for
539 assistance in reconstructing tomograms, as well as Adrian Nievergelt from the Gaia Pigino Group
540 at the Human Technopole Milano for his help processing cryo-EM tomograms with IsoNet. This
541 work was supported by the B CUBE of the TU Dresden, a German Federal Ministry of Education

542 and Research BMBF grant (to J.S., project 03Z22EN12), and a VW Foundation ''Life'' grant (to J.S.,
543 project 93090).
544

545 ## Materials and Methods

546 Cell Culture:

547 *M. mycoides* and JCVI-Syn3A were grown in liquid culture at 37ºC on a modified SP4 growth
548 medium with Phenol Red[73]. The lipid source was provided either by Fetal Bovine Serum (FBS),
549 complex natural source of mammalian lipids, or by complexing lipids with delipidated bovine
550 serum albumin (BSA). Lipids were dissolved in ethanol and added to the medium at 37ºC
551 immediately before the addition of cells, in the concentrations given in Table S1. *M. mycoides*
552 was passaged to new growth medium by adding 50 µL of cell culture at OD600 0.4-0.8 into 7 mL
553 of freshly prepared media in a T25 Flask (Stand., Vent. Cap) or 10mL of media in a Duran 100 mL
554 glass flask. This corresponded to roughly one passage per day. JCVI-Syn3A was passaged to new
555 medium by adding 200 µL of cell culture at OD600 0.2-0.6 into 7 mL of freshly prepared media.
556 This corresponded to one passage every two to four days, depending on cell growth rates. Cells
557 were grown at 37ºC and 40 RPM in a Kuhner shaker incubator.
558

559 Growth Rates:

560 Metabolic Growth Index

561 Due to differences in cell size and behavior between *M. mycoides* and JCVI-Syn3A, measuring
562 growth curves with optical density by taking the absorbance at 600 nm (OD_{600}) proved to be an
563 unreliable method to achieve growth estimates that were robustly comparable between the two
564 organisms. Phenol Red is a pH indicator that is commonly used as a readout for growth in
565 mycoplasma cell culture[74] as it detects changes in pH as metabolic activity acidifies the culture
566 media through absorbance at 562 nm (A_{562}). To obtain the rate of pH change (A_{562}) over time cells
567 were grown on the liquid handler system Biomek i7 Automated Workstation in 96-well plates
568 (square well, clear bottom, 400 uL media volume, 100 rpm shaking), and the absorbance was
569 recorded hourly to record changes in phenol red absorbance as cell growth acidifies the media
570 (Supplementary Fig. S3a)[19,73,74]. All absorbances were then plotted with respect to time, and then
571 fitted to the logistic function $N_t = K (1 + (K-N_0)/N_0) e^{-rt}$) where N_t is population at time t, K is the

572 carrying capacity, N_0 is the initial population size, and r is the growth rate; or, in this case, the
573 rate of pH change. Only the exponential part of the curve was considered to exclude lag and
574 stationary phase. To validate the relevance of this method as a readout for cell growth, growth
575 rates for a representative set of *M. mycoides* diets were calculated using OD_{600} and were
576 compared to the rates calculated with Phenol Red absorbance. The result was a strong linear
577 correlation between the two estimates (Supplementary Fig. S3b). Representative curves of the
578 entire period of growth for *M. Mycoides* and JCVI-Syn3B on three different diet and generated
579 by the two methods is also shown (Supplementary Fig S5). Cell growth data shown in
580 Supplementary Figure S5, measured by Phenol Red A_{562} and OD_{600} was obtained through hourly
581 manual measurements from cultures grown in 30 mL in a Duran 100 mL glass flask in a Kuhner
582 shaker incubator at 37ºC and 40 rpm shaking using a DeNovix Spectrophotometer.
583
584 Lipid Extraction and Thin Layer Chromatography:
585 Lipids were extracted using a Bligh-Dyer lipid extraction protocol[76]. When appropriate, lipid
586 concentration was determined with a phosphate assay. TLC plates with Silica Gel and a 10x
587 concentrating zone were pre-washed with chloroform to remove debris and other artifacts, and
588 were then dried at 60ºC for > 30 minutes to ensure complete solvent evaporation. Lipid samples
589 were then loaded on the plate and were dried at 60ºC for > 10 minutes to again ensure complete
590 solvent evaporation. The plate was then run in a closed glass chamber using a running solution
591 of Chloroform:Methanol:Acetic Acid:Water (85:25:5:4), and were subsequently dried again at
592 60ºC for > 30 minutes. TLC plates were then rinsed with a 3% Copper acetate and 8% phosphoric
593 acid solution and heated by a handheld heat gun at 280ºC to char lipid spots.
594
595 Liposome Preparation: Lipids of a known concentration (either in stock solutions or extracted
596 from cells and validated with a phosphate assay) were prepared in a 2 mL glass by having their
597 solvents evaporated overnight under a 10-17 mbar vacuum. Lipids were then resuspended in the
598 appropriate volume of Liposome buffer (LiB) (10 mM HEPES, 100 mM NaCl) to achieve 100 mM
599 liposome solution and incubated for 30 minutes at 37ºC. Subsequently, liposomes were

600 homogenized with ten freeze thaw cycles (1 minute in liquid nitrogen followed by 5 minutes at
601 60C) and 7 extrusion cycles in a Hamilton syringe setup through a 100 nm filter.
602
603 Propidium Iodide Osmotic Shock Assay: 3X 0.4 ODU of cells with OD 0.2-0.4 (1 ODU = 1 mL of cells
604 at OD 1) were harvested and spun down in pre-warmed centrifuge at 5000 g, 7minutes, 37ºC,
605 with slow acceleration slow deceleration. 1 µL of 1 mM Propidium Iodide dye was added to
606 appropriate wells on a black or clear bottom 96well plate. The supernatant was aspirated and
607 each cell pellet was resuspended in 400 µL of either H2O or 5X diluted mycoplasma wash buffer
608 (MWB) (original MWB: 20 mM HEPES, 200 mM NaCl, 1% W/V Glucose). An extra tube with cells
609 resuspended in 400 µL H2O and boiled at 95ºC in a thermoshaker at 1000 rpm for 10 minutes
610 was set up as a positive control. During that time, all other tubes were incubated on the 37ºC
611 thermoshaker at 600 rpm. 100 µL of the cells in the appropriate buffer was added to each of their
612 three analytical wells on the 96 well plate. Cells were incubated for 30 minutes with shaking at
613 37ºC in a TECAN Spark 20M plate reader and the fluorescent signal was subsequently measured
614 at excitation 539 nm emission 619 nm.
615
616 Fluorescein Diacetate Permeability Assay: 3X 0.4 ODU of cells with OD 0.2-0.4 were harvested
617 and spun down in pre-warmed centrifuge at 5000 g, 7minutes, 37ºC, with slow acceleration slow
618 deceleration. Cells were washed 1x in MWB and resuspended in 400 µL MWB. A Fluorescein
619 Standard curve was prepared on the plate in the following concentrations: 0, 0.25 ,0.5, 1.2, 2 µM
620 Fluorescein. 100 µL resuspended cells were added to the proper wells (in triplicate), and 100 µL
621 MWB was added to the Fluorescein standard wells. FDA was added to cell wells to achieve final
622 FDA concentration of 5 µM. Cells were incubated on the TECAN Spark 20M at 37ºC for 140
623 minutes and measurements were taken every 20 minutes at excitation 485 and emission 525.
624 The permeability coefficient (P) of FDA was calculated using Fick's Law ($Q = P*A*(C_{out} - Ci_n)$) where
625 Q is the flux across the membrane, and is a constant as the slope of fluorescein increase over
626 time was linear; A is the area of the membrane, calculated using the assumption that the cross
627 sectional area of POPC + Cholesterol in a bilayer is 45.1 Å[77], the ratio of POPC : Cholesterol is
628 roughly 1:1, the area of POPC + cholesterol is equivalent to the area of Enantiomeric POPC +

629 Cholesterol, and the number of POPC molecules can be calculated from the phosphate assay
630 described below; C_{out} and C_{in} are the concentrations of FDA outside and inside the cell
631 (respectively); and Ci_n is 0 as FDA is immediately converted to fluorescein upon entering the cell.
632
633 C-Laurdan General Polarization Assay: Liposomes from whole cell lipid extracts were incubated
634 at 37ºc and 1000 rpm for 10 minutes on a tabletop thermoshaker. While cells were incubating,
635 c-Laurdan was removed from a -20ºc freezer and warmed to room temperature on the bench. 1
636 mM c-Laurdan stock in EtOH was diluted 4x and 1 uL of diluted stock for a final molarity 0.5 µM
637 C-Laurdan was added to 500 µL of liposomes. Samples were incubated at 37ºc and 1000 rpm
638 shaking for 10 minutes on a tabletop thermoshaker. 100 µL of each sample was added to a flat
639 bottom 96 well plate well with analytical triplicates for each biological replicate. The signal was
640 measured on a TECAN Spark 20M with a 2 channel fluorescence reading with excitation at 385nm
641 and emission at 440 and 490 nm respectively. General polarization (GP) was calculated using the
642 formula: GP = (I440 - I490) / (I440 + I490) where I is the fluorescence emission intensity at the
643 respective wavelength.
644
645 Phosphate Assay: To estimate the concentration of phospholipids in a certain amount of cells,
646 the amount of phosphate in the lipid extraction of 1 OD Unit (ODU: 1mL of OD_{600} = 1) of cells was
647 measured. To measure phosphate amount a modified version of the method of Chen et al. was
648 used[78]. The lipid extraction was added to glass pyrex tubes with both biological and analytical
649 triplicates (3 vials per biological replicate), and the solvent was evaporated by a brief (<5 minute)
650 incubation at 200ºC. 50 µL of water were added to each sample. To prepare a standard curve of
651 phosphate amounts, an ICP Phosphorus standard was diluted in water to give 5, 10, 20, 50 and
652 100, and 200 nmols of phosphate. 500 µL of 70% perchloric acid was added to each vial and, after
653 brief vortexing, samples were incubated at 200ºC for 120 minutes. Tubes were cooled down in
654 ice water, and 1mL of 10% w/v ascorbic acid followed immediately by 1 mL of 2.5% w/v
655 ammonium heptamolybdate were added (with a brief vortex after adding each reagent). Samples
656 were incubated at 37ºC for 30 minutes, and then absorbance at 820 nm was measured on a
657 TECAN Spark 20M plate reader by adding 200 µL of each tube to a clear bottom 96 well plate . A

658 standard curve of absorbance at 820 vs phosphate amount was calculated using the phosphate
659 standard, and lipid amount of each sample was calculated based on the absorbance value,
660 standard curve, and assumption that one phosphate molecule equals one phospholipid.
661
662 Lipidomic Analysis: Lipids extracted from cells using the aforementioned Bligh-Dyer protocol
663 were submitted to Lipotype for mass spectrometry based analysis[79]. The general procedure is
664 described in Sampaio et.al, 2011[2]. For the analysis, samples were spiked with internal lipid
665 standard mixture containing: cardiolipin 14:0/14:0/14:0/14:0, ceramide 18:1;2/17:0,
666 diacylglycerol 17:0/17:0, hexosylceramide 18:1;2/12:0, lyso-phosphatidate 17:0, lyso-
667 phosphatidylcholine 12:0, lyso-phosphatidylethanolamine 17:1, lyso-phosphatidylglycerol 17:1,
668 lyso-phosphatidylinositol 17:1, lyso-phosphatidylserine 17:1, phosphatidate 17:0/17:0,
669 phosphatidylcholine 17:0/17:0, phosphatidylethanolamine 17:0/17:0, phosphatidylglycerol
670 17:0/17:0, phosphatidylinositol 16:0/16:0, phosphatidylserine 17:0/17:0, cholesterol ester 20:0,
671 sphingomyelin 18:1;2/12:0;0, triacylglycerol 17:0/17:0/17:0, and cholesterol D6. After extraction,
672 the organic phase was transferred to an infusion plate and dried in a speed vacuum concentrator.
673 It was then resuspended in 7.5 mM ammonium acetate in chloroform/methanol/propanol (1:2:4,
674 V:V:V) and a 33% ethanol solution of methylamine in chloroform/methanol (0.003:5:1; V:V:V).
675 All liquid handling steps were performed using Hamilton Robotics STARlet robotic platform with
676 the Anti Droplet Control feature for organic solvents pipetting. Samples were analyzed by direct
677 infusion on a QExactive mass spectrometer (Thermo Scientific) equipped with a TriVersa
678 NanoMate ion source (Advion Biosciences). Samples were analyzed in both positive and negative
679 ion modes with a resolution of Rm/z=200=280000 for MS and Rm/z=200=17500 for MSMS
680 experiments, in a single acquisition. MSMS was triggered by an inclusion list encompassing
681 corresponding MS mass ranges scanned in 1 Da increments. Both MS and MSMS data were
682 combined to monitor CE, DAG and TAG ions as ammonium adducts; PC, PC O-, and Diether PC as
683 acetate adducts; and CL, PA, PE, PE O-, PG, PI and PS as deprotonated anions. MS only was used
684 to monitor LPA, LPE, LPE O-, LPI and LPS as deprotonated anions; ceramide, hexosylceramide,
685 sphingomyelin, LPC and LPC O- as acetate adducts and cholesterol as an ammonium adduct of an
686 acetylated derivative[80].

687

688 Room temperature TEM:

689 JCVI-Syn3A cells were adapted to FBS, POPC + Cholesterol, and D.PC + Cholesterol diets and
690 harvested at between OD_{600} 0.05-0.2 at volumes to achieve 1ODU of cells for each diet. Cells
691 were spun down and resuspended in 1mL Mycoplasma Wash Buffer without glucose (20mM
692 HEPES, 200 mM NaCl). Cells were pre-fixed 30 min at room temperature with a final
693 concentration of 0.5% glutaraldehyde (25% aqueous stock solution (EMS), directly added to the
694 culture medium). Then cells were spun down for 7 min @ 7000 g @ 37°C in a centrifuge (Heraeus
695 Biofuge PrimoR with swingout buckets). The cell pellet was sucked into cellulose capillary tubes
696 with an inner diameter of 200 µm and a permeability cut-off >5 KD (Leica). Filled capillaries were
697 chopped into small pieces with a scalpel blade, at the same time sealing the capillary ends.
698 Capillary pieces were rapidly frozen using Leica EM-ICE high pressure freezing device in 6 mm–
699 aluminum carriers with 200 µm deep depression (Leica) using hexadecene as a filler. Freeze
700 substitution was done in an AFS 2 freeze substitution device (Leica) in 1% osmium tetroxide in
701 acetone starting at -90 °C and raising the temperature to 0° C over 72 hrs. Samples were
702 infiltrated gradually with 25%, 50%, 75%, 100% EMbed 812 (Science Services) in acetone over
703 two days. Capillaries were infiltrated with pure resin over two days and embedded in double end
704 silicon molds (TED PELLA INC) and polymerized at 60 °C for 48 hrs. 70 nm–sections were cut with
705 a Leica EM UC6 and mounted on formvar-coated copper slot grids (EMS). Sections on the grids
706 were contrasted with uranyl acetate and lead citrate prior to imaging. Imaging was done on a
707 Tecnai T12 (Thermo Fisher Scientific (formerly FEI), Hillsboro, Oregon, USA) transmission electron
708 microscope at 100 kV acceleration voltage. The images were acquired with a F416 camera (Tietz
709 Video and Image Processing Systems GmbH, Gilching, Germany) at 4096x4096 pixels using
710 SerialEM software. Before taking an image, the sample was automatically exposed to the beam
711 for 0.5-2 seconds to reduce drift. The exposure time (between 0.5 and 1.5 seconds) was
712 subdivided into 3 subframes which were then automatically aligned by cross correlation and
713 added up in order to form the final image in order to reduce image blurring by sample drift.

714

715 *Cryo TEM*:

716 JCVI-Syn3A cells were adapted to FBS, POPC + Cholesterol, and D.PC + Cholesterol diets and
717 harvested at between OD_{600} 0.05-0.2 (mid-exponential growth phase) at volumes to achieve
718 1ODU of cells for each diet. Short before freezing, cells were spun down and resuspended in 1
719 mL Mycoplasma wash buffer without glucose (20 mM HEPES, 200 mM NaCl). Quantifoil 2.1
720 copper 200 mesh grids were cleaned with chloroform before usage. Glow discharging was
721 performed on a PELCO Easy glow for 30 seconds, 15 mA on both sides of the grid. 2 µl of sample
722 being added to both sides of the grid, 1 µl of gold (Protein A gold, PAG 10, pre-diluted 1:25 was
723 added to the carbon side only. Cryo fixation was performed by plunge freezing in liquid Ethane
724 using a Leica GP with humidity chamber set to 21 ˚C, a humidity of 98 % and a blotting time of 5
725 seconds from the back of the grid with Whatmann paper No 1. Frozen grids were stored in liquid
726 nitrogen[81].
727
728 Cryo-electron tomography was done on a Titan Halo transmission electron microscope with field
729 emission gun electron source and a Gatan K2 Summit direct electron detector at 300 kV with an
730 energy filter using a slit width of 20 eV. Full grid overview was acquired with SerialEM by
731 automatically acquiring and stitching low-magnification (×210) images. Tilt series was taken with
732 SerialEM on areas of interest at ×30,000 nominal image magnification, calibrated pixel size of
733 2.36 Å (super-resolution mode) and 2° increments with a bidirectional tilt scheme from 20° to -
734 58° and from 22° to 58°. The acquisition was done with a defocus target of 5 µm and the
735 accumulative dose was 80 - 90 e− per Å2 per tomogram. Images were acquired in dose
736 fractionation mode with frame times between 0.10 and 0.25 s. Correction of the sample motion
737 induced by the electron beam was done with MotionCor. Tomogram reconstruction was
738 performed using Etomo from IMOD 4.11.18 using weighted back projection. Contrast transfer
739 function curves were estimated with Ctfplotter and corrected by phase-flipping with the software
740 Ctfphaseflip, both implemented in IMOD. Dose-weighted filtering was performed by using the
741 mtffilter implemented in IMOD. To enhance the contrast of macromolecular structures and fill
742 up missing wedge information IsoNet was used. Visualization of tomograms and averaged
743 electron density maps was performed in 3dmod from IMOD[82]. Computer visualization of three-
744 dimensional image data using IMOD. J. Struct. Biol. 116:71-76.); rendering of isosurfaces and

745 structure fitting was performed using UCSF ChimeraX 1.8, developed by the Resource for
746 Biocomputing, Visualization, and Informatics at the University of California, San Francisco, with
747 support from National Institutes of Health R01-GM129325 and the Office of Cyber Infrastructure
748 and Computational Biology, National Institute of Allergy and Infectious Diseases.
749
750 Statistical Analysis
751 For growth rate calculations in Figures 3, 4, and 5 the number of biological and analytical
752 replicates is given in Table S1. For the propidium iodide assays in Figure 5 there are three
753 biological replicates each with three analytical replicates. For the FDA assay in Figure 5 there are
754 three biological replicates each with three analytical replicates. For the c-Laurdan assay in Figure
755 6 there are three biological replicates each with three analytical replicates. Statistical significance
756 was calculated with an unpaired t-test. All error bars indicate the mean +/- the standard
757 deviation.
758
759 Materials:
760 SP4 (For 1 L):
761 PPLO (3.5 g) (Becton, Dickinson, and Company product no. 255420)
762 Tryptone (10 g) (Sigma product no 70169)
763 Peptone (5 g) (Sigma product no 70176)
764 20% Glucose (25 mL) (Ross product no. X997.2)
765 20% Yeastolate (10 mL) (Becton, Dickinson, and Company product no. 255772)
766 15% Yeast Extract (35 mL) (Roth product no. 2904.3)
767 70g/L BSA (85 mL) (Sigma product no. A7030) or FBS (170 mL) (Biowest Product
768 no. 5181H-500)
769 400,000U/mL Penicillin G-sodium salt (2.5 mL) (Roth product no. HP48.1)
770 10 mg/mL L-Glutamate (5 mL) (Roth product no. HN08.2)
771 Sodium Bicarbonate (1.04 g) (Honeywell product no. 71630)
772 CMRL (4.9 g) (US Biological Lifesciences product no. C5900)
773 Phenol Red (11 mg) (Sigma product no. P3532)

774

775 Lipids:

776 Cholesterol (Avanti product no. 700100)

777 Diether POPC (Diether 1-palmitoyl-2-oleoyl-glycero-3-phosphocholine) (Avanti
778 product no. 999983)

779 Diether DPPC (Diether 1-palmitoyl-2-palmitoyl-glycero-3-phosphocholine) (Avanti
780 product no. 999992)

781 Diether DOPC (Diether 1-oleoyl-2-oleoyl-glycero-3-phosphocholine) (Avanti
782 product no. 999991)

783 Diether POPG (Diether 1-palmitoyl-2-oleoyl-glycero-3-phosphotdylglycerol)
784 (Avanti product no. 999973)

785 POPC (1-palmitoyl-2-oleoyl-glycero-3-phosphocholine) (Avanti product no.
786 850457)

787 DPPC (1-palmitoyl-2-palmitoyl-glycero-3-phosphocholine) (Avanti product no.
788 850355)

789 DOPC (1-oleoyl-2-oleoyl-glycero-3-phosphocholine) (Avanti product no. 850375)

790 POPG (1-palmitoyl-2-oleoyl-glycero-3-phosphotdylglycerol) (Avanti product no.
791 840457)

792 DPPG (1-palmitoyl-2-palmitoyl-glycero-3-phosphoglycerol) (Avanti product no.
793 840455)

794 DOPG (1-oleoyl-2-oleoyl-glycero-3-phosphoglycerol) (Avanti product no. 850475)

795 POPE (1-palmitoyl-2-oleoyl-glycero-3-phosphoethanolamine) (Avanti product no.
796 850757)

797

798 DPPE (1-palmitoyl-2-palmitoyl-glycero-3-phosphoethanolamine) (Avanti product
799 no. 850705)

800 DOPE (1-oleoyl-2-oleoyl-glycero-3-phosphoethanolamine) (Avanti product no.
801 850725)

802 Oleic Acid (c*is*-9-Octadecenoic acid) (Sigma product no. 01383)

803 Palmitic Acid (1-Pentadecanecarboxylic acid) (Sigma P0500)

804 Enantiomeric POPC (3-palmitoyl-2-oleoyl-glycero-1-phosphocholine) (Avanti
805 product no. 850855)

806 16-0 Cardiolipin (1',3'-bis[1,2-dipalmitoyl-sn-glycero-3-phospho]-glycerol) (Avanti
807 product no. 710333)

808

809 Assays:

810 FDA (Sigma product no. F7378)

811 Fluorescein (Fluka product no. 28803)

812 Propidium Iodide (Sigma product no. 537059)

813 C-Laurdan (Stratech Scientific Ltd. product no. T0001-SFC-1)

814

815 Cells:

816 JCVI-Syn3A-*mCherry (*From Telesis Bio)

817 *Mycoplasma mycoides subspecies capri strain GM12 (*From Telesis Bio)

818

819 Machines:

820 TECAN Spark 20M with Te-Cool cooling module

821 Biomek i7 Automated Workstation

822 DeNovix DS-11 FX +

823 PicoQuant FluoTime 300 High Performance Fluorescence Lifetime and Steady
824 State Spectrometer

825

826 **Data Availability Statement:**
827 The lipidomic datasets generated in this study have been uploaded to the Zenodo repository
828 and can be found at the DOI: 10.5281/zenodo.13817894. Due to proprietary restrictions
829 imposed by the data provider, Lipotype GmbH, raw lipidomics instrument files cannot be
830 deposited in a standard metabolomics repository, as they contain commercially sensitive
831 information. The TEM data has been deposited in the EBI Biolibraries repository and can be
832 found at the DOI: 10.6019/S-BSST1651. The cryoEM data has been deposited in the Electron
833 Microscopy Data Bank (EMDB) within the pDBE database, and can be found with the accession

codes: EMD-51614, EMD-51606, EMD-51607, EMD-51608, EMD-51609, and EMD-51610. All other source data are provided with this paper.

Citations

1. Chwastek, G. *et al.* Principles of Membrane Adaptation Revealed through Environmentally Induced Bacterial Lipidome Remodeling. *Cell Rep.* **32**, 108165 (2020).
2. Sampaio, J. L. *et al.* Membrane lipidome of an epithelial cell line. *Proc. Natl. Acad. Sci. U. S. A.* **108**, 1903–1907 (2011).
3. Melero, A. & Jiménez-Rojo, N. Cracking the membrane lipid code. *Curr. Opin. Cell Biol.* **83**, 102203 (2023).
4. Harayama, T. & Riezman, H. Understanding the diversity of membrane lipid composition. *Nat. Rev. Mol. Cell Biol.* **19**, 281–296 (2018).
5. Klose, C. *et al.* Flexibility of a Eukaryotic Lipidome – Insights from Yeast Lipidomics. *PLoS ONE* **7**, e35063 (2012).
6. Safronova, N., Junghans, L. & Saenz, J. P. Temperature change elicits lipidome adaptation in the simple organisms Mycoplasma mycoides and JCVI-syn3B. *Cell Rep.* **43**, (2024).
7. Dowhan, W. A retrospective: Use of Escherichia coli as a vehicle to study phospholipid synthesis and function. *Biochim. Biophys. Acta BBA - Mol. Cell Biol. Lipids* **1831**, 471–494 (2013).
8. Cronan, J. E. & Gelmann, E. P. An Estimate of the Minimum Amount of Unsaturated Fatty Acid Required for Growth of Escherichia coli. *J. Biol. Chem.* **248**, 1188–1195 (1973).
9. Boudreaux, D. P., Freese, E., Eisenstadt, E. & Iijima, T. Biochemical and Genetic Characterization of an Auxotroph of Bacillus subtilis Altered in the Acyl-CoA:Acyl-Carrier-Protein Transacylase. *Eur. J. Biochem.* **115**, 175–182 (1981).
10. Budin, I. *et al.* Viscous control of cellular respiration by membrane lipid composition. *Sci. N. Y. NY* **248**, eaat7925 (2018).
11. Gohrbandt, M. *et al.* Low membrane fluidity triggers lipid phase separation and protein segregation in living bacteria. *EMBO J.* **41**, e109800 (2022).
12. Willdigg, J. R. & Helmann, J. D. Mini Review: Bacterial Membrane Composition and Its Modulation in Response to Stress. *Front. Mol. Biosci.* **8**, (2021).
13. Salzberg, L. I. & Helmann, J. D. Phenotypic and Transcriptomic Characterization of Bacillus subtilis Mutants with Grossly Altered Membrane Composition▿ †. *J. Bacteriol.* **190**, 7797–7807 (2008).
14. Rottem, S. & Kahane, I. *Mycoplasma Cell Membranes*. (Springer Science & Business Media, 2012).
15. Kornspan, J. D. & Rottem, S. The Phospholipid Profile of Mycoplasmas. *J. Lipids* **2012**, 640762 (2012).
16. McElhaney, R. N. Physical Studies of Lipid Organization and Dynamics in Mycoplasma Membranes. in *Mycoplasma Cell Membranes* (eds. Rottem, S. & Kahane, I.) 53–108 (Springer US, Boston, MA, 1993). doi:10.1007/978-1-4615-2924-8_3.
17. Bittman, R. Mycoplasma Membrane Lipids Chemical Composition and Transbilayer Distribution. in *Mycoplasma Cell Membranes* (eds. Rottem, S. & Kahane, I.) 29–52 (Springer US, Boston, MA, 1993). doi:10.1007/978-1-4615-2924-8_2.

877 18. Razin, S., Yogev, D. & Naot, Y. Molecular biology and pathogenicity of mycoplasmas.
878 *Microbiol. Mol. Biol. Rev.* **62**, 1094-+ (1998).
879 19. Gaspari, E. *et al.* Model-driven design allows growth of Mycoplasma pneumoniae on
880 serum-free media. *Npj Syst. Biol. Appl.* **6**, 1–11 (2020).
881 20. Hutchison, C. A. *et al.* Design and synthesis of a minimal bacterial genome. *Sci. N. Y. NY*
882 **351**, aad6253–aad6253 (2016).
883 21. Pelletier, J. F. *et al.* Genetic requirements for cell division in a genomically minimal cell.
884 *Cell* **184**, 2430-2440.e16 (2021).
885 22. Lartigue, C. *et al.* Creating bacterial strains from genomes that have been cloned and
886 engineered in yeast. *Science* **325**, 1693–1696 (2009).
887 23. Rottem, S., Yashouv, J., Ne'eman, Z. & Razin, S. Cholesterol in mycoplasma membranes.
888 Composition, ultrastructure and biological properties of membranes from *Mycoplasma*
889 *mycoides* var. *capri* cells adapted to grow with low cholesterol concentrations. *Biochim.*
890 *Biophys. Acta BBA - Biomembr.* **323**, 495–508 (1973).
891 24. Archer, D. B. Y. 1975. Modification of the Membrane Composition of Mycoplasma
892 mycoides subsp. capri by the Growth Medium. *Microbiology* **88**, 329–338.
893 25. Dahl, J. Uptake of fatty acids by Mycoplasma capricolum. *J. Bacteriol.* **170**, 2022–2026
894 (1988).
895 26. Razin, S., Efrati, H., Kutner, S. & Rottem, S. Cholesterol and Phospholipid Uptake by
896 Mycoplasmas. *Rev. Infect. Dis.* **4**, S85–S92 (1982).
897 27. Plackett, P. The Synthesis of Polar Lipids by Mycoplasma. *Ann. N. Y. Acad. Sci.* **143**, 158–
898 164 (1967).
899 28. Salman, M. & Rottem, S. The cell membrane of *Mycoplasma penetrans*: lipid
900 composition and phospholipase A1 activity. *Biochim. Biophys. Acta BBA - Biomembr.* **1235**, 369–
901 377 (1995).
902 29. Bhandari, S. & Asnani, P. J. Characterization of phospholipase A2 of mycoplasma species.
903 *Folia Microbiol. (Praha)* **34**, 294–301 (1989).
904 30. Rottem, S., Adar, L., Gross, Z., Ne'eman, Z. & Davis, P. J. Incorporation and modification
905 of exogenous phosphatidylcholines by mycoplasmas. *J. Bacteriol.* **167**, 299–304 (1986).
906 31. Rottem, S. Membrane lipids of mycoplasmas. *Biochim. Biophys. Acta BBA - Biomembr.*
907 **604**, 65–90 (1980).
908 32. Rottem, S. & Markowitz, O. Membrane lipids of Mycoplasma gallisepticum: a
909 disaturated phosphatidylcholine and a phosphatidylglycerol with an unusual positional
910 distribution of fatty acids. *Biochemistry* **18**, 2930–2935 (1979).
911 33. Thornburg, Z. R. *et al.* Fundamental behaviors emerge from simulations of a living
912 minimal cell. *Cell* **185**, 345-360.e28 (2022).
913 34. Gross, Z. & Rottem, S. Lipid interconversions in aging Mycoplasma capricolum cultures.
914 *J. Bacteriol.* **167**, 986–991 (1986).
915 35. Razin, S. Sterols in Mycoplasma Membranes. in *Current Topics in Membranes and*
916 *Transport* (eds. Bronner, F. & Kleinteller, A.) vol. 17 183–205 (Academic Press, 1982).
917 36. Dahl, J. The Role of Cholesterol in Mycoplasma Membranes. in *Mycoplasma Cell*
918 *Membranes* (eds. Rottem, S. & Kahane, I.) 167–188 (Springer US, Boston, MA, 1993).
919 doi:10.1007/978-1-4615-2924-8_5.

920 37. van Meer, G., Voelker, D. R. & Feigenson, G. W. Membrane lipids: where they are and
921 how they behave. *Nat. Rev. Mol. Cell Biol.* **9**, 112–124 (2008).
922 38. Janmey, P. A. & Kinnunen, P. K. J. Biophysical properties of lipids and dynamic
923 membranes. *Trends Cell Biol.* **16**, 538–546 (2006).
924 39. Winnikoff, J. R. *et al.* Homeocurvature adaptation of phospholipids to pressure in deep-
925 sea invertebrates. *Science* **384**, 1482–1488 (2024).
926 40. Mouritsen, O. G. & Zuckermann, M. J. What's so special about cholesterol? *Lipids* **39**,
927 1101–1113 (2004).
928 41. Varma, M. & Deserno, M. Distribution of cholesterol in asymmetric membranes driven
929 by composition and differential stress. *Biophys. J.* **121**, 4001–4018 (2022).
930 42. Rangholia, N., Leisner, T. M. & Holly, S. P. Bioactive Ether Lipids: Primordial Modulators
931 of Cellular Signaling. *Metabolites* **11**, 41 (2021).
932 43. Choquet, C. G., Patel, G. B., Sprott, G. D. & Beveridge, T. J. Stability of pressure-extruded
933 liposomes made from archaeobacterial ether lipids. *Appl. Microbiol. Biotechnol.* **42**, 375–384
934 (1994).
935 44. Safronova, N., Junghans, L. & Saenz, J. P. Temperature change elicits lipidome
936 adaptation in the simple organisms Mycoplasma mycoides and JCVI-syn3B. *Cell Rep.* **43**, (2024).
937 45. Breuer, M. *et al.* Essential metabolism for a minimal cell. *eLife* **8**, e36842 (2019).
938 46. Sakai, A. *et al.* Traditional protocols and optimization methods lead to absent expression
939 in a mycoplasma cell-free gene expression platform. *Synth. Biol.* **7**, ysac008 (2022).
940 47. Bianchi, D. M., Pelletier, J. F., Hutchison, C. A., Glass, J. I. & Luthey-Schulten, Z. Toward
941 the Complete Functional Characterization of a Minimal Bacterial Proteome. *J. Phys. Chem. B*
942 **126**, 6820–6834 (2022).
943 48. Studer, P. *et al.* Proliferation of Listeria monocytogenes L-form cells by formation of
944 internal and external vesicles. *Nat. Commun.* **7**, 13631 (2016).
945 49. van Wolferen, M., Pulschen, A. A., Baum, B., Gribaldo, S. & Albers, S.-V. The cell biology
946 of archaea. *Nat. Microbiol.* **7**, 1744–1755 (2022).
947 50. Altamura, E. *et al.* Racemic Phospholipids for Origin of Life Studies. *Symmetry* **12**, 1108
948 (2020).
949 51. Villanueva, L. *et al.* Bridging the membrane lipid divide: bacteria of the FCB group
950 superphylum have the potential to synthesize archaeal ether lipids. *ISME J.* **15**, 168–182 (2021).
951 52. Martin, H. S., Podolsky, K. A. & Devaraj, N. K. Probing the Role of Chirality in
952 Phospholipid Membranes. *ChemBioChem* **22**, 3148–3157 (2021).
953 53. Sojo, V. Why the Lipid Divide? Membrane Proteins as Drivers of the Split between the
954 Lipids of the Three Domains of Life. *BioEssays* **41**, 1800251 (2019).
955 54. Caforio, A. *et al.* Converting Escherichia coli into an archaebacterium with a hybrid
956 heterochiral membrane. *Proc. Natl. Acad. Sci.* **115**, 3704–3709 (2018).
957 55. Brown, M. B., Stoll, M., Maxwell, J. & Senior, D. F. Survival of feline mycoplasmas in
958 urine. *J. Clin. Microbiol.* **29**, 1078–1080 (1991).
959 56. Rizk, S. *et al.* Functional diversity of isoprenoid lipids in Methylobacterium extorquens
960 PA1. *Mol. Microbiol.* (2021) doi:10.1111/mmi.14794.
961 57. Levental, K. R. *et al.* Lipidomic and biophysical homeostasis of mammalian membranes
962 counteracts dietary lipid perturbations to maintain cellular fitness. *Nat. Commun.* **11**, 1339
963 (2020).

964 58. Parasassi, T., Stasio, G. de, Ravagnan, G., Rusch, R. M. & Gratton, E. Quantitation of lipid
965 phases in phospholipid vesicles by the generalized polarization of Laurdan fluorescence.
966 *Biophys. J.* **60**, 179–189 (1991).
967 59. Steinkühler, J., Sezgin, E., Urbančič, I., Eggeling, C. & Dimova, R. Mechanical properties
968 of plasma membrane vesicles correlate with lipid order, viscosity and cell density. *Commun.*
969 *Biol.* **2**, 337–8 (2019).
970 60. Chen, L. *et al.* Chiral Selective Transmembrane Transport of Amino Acids through
971 Artificial Channels. *J. Am. Chem. Soc.* **135**, 2152–2155 (2013).
972 61. Ishigami, T., Suga, K. & Umakoshi, H. Chiral Recognition of l-Amino Acids on Liposomes
973 Prepared with l-Phospholipid. *ACS Appl. Mater. Interfaces* **7**, 21065–21072 (2015).
974 62. Dowhan, W. Molecular genetic approaches to defining lipid function. *J. Lipid Res.* **50**,
975 S305–S310 (2009).
976 63. Dowhan, W. & Bogdanov, M. Molecular genetic and biochemical approaches for
977 defining lipid-dependent membrane protein folding. *Biochim. Biophys. Acta BBA - Biomembr.*
978 **1818**, 1097–1107 (2012).
979 64. Romanauska, A. & Köhler, A. Lipid saturation controls nuclear envelope function. *Nat.*
980 *Cell Biol.* **25**, 1290–1302 (2023).
981 65. Manni, M. M. *et al.* Acyl chain asymmetry and polyunsaturation of brain phospholipids
982 facilitate membrane vesiculation without leakage. *eLife* **7**, e34394 (2018).
983 66. Nguyen, H. N. A., Sharp, L., Lyman, E. & Saenz, J. P. Varying the position of phospholipid
984 acyl chain unsaturation modulates hopanoid and sterol ordering. *Biophys. J.* **123**, 1896–1902
985 (2024).
986 67. Mccoy, R. E. *et al.* Acholeplasma florum, a New Species Isolated from Plants†. *Int. J. Syst.*
987 *Evol. Microbiol.* **34**, 11–15 (1984).
988 68. Matteau, D. *et al.* Integrative characterization of the near-minimal bacterium
989 Mesoplasma florum. *Mol. Syst. Biol.* **16**, e9844 (2020).
990 69. Koga, Y., Kyuragi, T., Nishihara, M. & Sone, N. Did Archaeal and Bacterial Cells Arise
991 Independently from Noncellular Precursors? A Hypothesis Stating That the Advent of
992 Membrane Phospholipid with Enantiomeric Glycerophosphate Backbones Caused the
993 Separation of the Two Lines of Descent. *J. Mol. Evol.* **46**, 54–63 (1998).
994 70. Koga, Y. Early Evolution of Membrane Lipids: How did the Lipid Divide Occur? *J. Mol.*
995 *Evol.* **72**, 274–282 (2011).
996 71. Matsumi, R., Atomi, H., Driessen, A. J. M. & van der Oost, J. Isoprenoid biosynthesis in
997 Archaea – Biochemical and evolutionary implications. *Res. Microbiol.* **162**, 39–52 (2011).
998 72. Koonin, E. V. Archaeal ancestors of eukaryotes: not so elusive any more. *BMC Biol.* **13**,
999 84 (2015).
1000 73. Fritz, B. A., Thomas, C. B., Van Ess, P. & Yuill, T. M. Comparison of a Modified Edward-
1001 Type Medium and a Modified SP4-Type Medium for Primary Isolation of Mycoplasma
1002 gallisepticum (MG) from Chickens Vaccinated with the F Strain of MG. *Avian Dis.* **35**, 591–598
1003 (1991).
1004 74. Low, I. E. & Eaton, M. D. Replication of Mycoplasma pneumoniae in Broth Culture. *J.*
1005 *Bacteriol.* **89**, 725–728 (1965).
1006 75. Meur, S. k., Sikdar, A., Srivastava, N. c. & Srivastava, S. k. Rapid photometric assay of
1007 growth of Mycoplasma mycoides subsp. capri. *J. Appl. Bacteriol.* **66**, 301–302 (1989).

1008 76. Bligh, E. G. & Dyer, W. J. A Rapid Method of Total Lipid Extraction and Purification. *Can.*
1009 *J. Biochem. Physiol.* **37**, 911–917 (1959).
1010 77. Leftin, A., Molugu, T. R., Job, C., Beyer, K. & Brown, M. F. Area per Lipid and Cholesterol
1011 Interactions in Membranes from Separated Local-Field 13C NMR Spectroscopy. *Biophys. J.* **107**,
1012 2274–2286 (2014).
1013 78. Chen, P. S., Toribara, T. Y. & Warner, H. Microdetermination of Phosphorus. *Analytical*
1014 *Chemistry* **28***,* 1756-1758 (1956).
1015 79. Ejsing, C. S. *et al.* Global analysis of the yeast lipidome by quantitative shotgun mass
1016 spectrometry. *Proc. Natl. Acad. Sci.* **106**, 2136–2141 (2009).
1017 80. Liebisch, G. *et al.* High throughput quantification of cholesterol and cholesteryl ester by
1018 electrospray ionization tandem mass spectrometry (ESI-MS/MS). *Biochim. Biophys. Acta BBA -*
1019 *Mol. Cell Biol. Lipids* **1761**, 121–128 (2006).
1020 81. Gilbert, B. R. *et al.* Generating Chromosome Geometries in a Minimal Cell From Cryo-
1021 Electron Tomograms and Chromosome Conformation Capture Maps. *Front. Mol. Biosci.* **8**,
1022 (2021).
1023 82. Kremer, J. R., Mastronarde, D. N. & McIntosh, J. R. Computer Visualization of Three-
1024 Dimensional Image Data Using IMOD. *J. Struct. Biol.* **116**, 71–76 (1996).
1025
1026

Table 1 - Lipid Names and Abbreviations			
Lipid Class Name	**Lipid Class Abbreviation**	**Lipid Species Name**	**Lipid Species Abbreviation**
Sterol	N/A	Cholesterol	N/A
Diether Phosphatidylcholine	diether PC	1-O-hexadecanyl-2-O-(9Z-octadecenyl)-sn-glycero-3-phosphocholine	diether PC
Diether Phosphatidylglycerol	diether PG	1-O-hexadecanyl-2-O-(9Z-octadecenyl)-sn-glycero-3-phospho-(1'-rac-glycerol)	diether PG
Diether Phosphatidylethanolamine	diether PE	1-O-hexadecanyl-2-O-(9Z-octadecenyl)-sn-glycero-3-phosphoethanolamine	diether PE
Phosphatidylcholine	PC	1-palmitoyl-2-oleoyl-glycero-3-phosphocholine	POPC
		1,2-dipalmitoyl-sn-glycero-3-phosphocholine	DPPC
		1,2-dioleoyl-sn-glycero-3-phosphocholine	DOPC
Phosphatidylglycerol	PG	1-palmitoyl-2-oleoyl-sn-glycero-3-phospho-(1'-rac-glycerol)	POPG
		1,2-dipalmitoyl-sn-glycero-3-phospho-(1'-rac-glycerol)	DPPG
		1,2-dioleoyl-sn-glycero-3-phospho-(1'-rac-glycerol)	DOPG
Phosphatidylethanolamine	PE	1-palmitoyl-2-oleoyl-sn-glycero-3-phosphoethanolamine	POPE
		1,2-dipalmitoyl-sn-glycero-3-phosphoethanolamine	DPPE
		1,2-dioleoyl-sn-glycero-3-phosphoethanolamine	DOPE
Fatty Acids	FA	(9Z)-Octadec-9-enoic acid	Oleic Acid
		Hexadecanoic acid	Palmitic Acid
Enantiomeric Phosphatidylcholine	Ent PC	3-palmitoyl-2-oleoyl-sn-glycero-1-phosphocholine	Enantiomeric POPC
Phosphatidic acid	PA	1-palmitoyl-2-oleoyl-sn-glycero-3-phosphate	POPA
Cardiolipin	CL	1',3'-bis[1,2-dipalmitoyl-sn-glycero-3-phospho]-glycerol	16:0 Cardiolipin
		1',3'-bis[1-palmitoyl-2-oleoyl-sn-glycero-3-phospho]-glycerol	16:0-18:1 Cardiolipin
Sphingomyelin	SM	N/A	N/A
Lyso-Phosphatidylcholine	Lyso PC	1-oleoyl-2-hydroxy-sn-glycero-3-phosphocholine	18:1-Lyso PC
		1-palmitoyl-2-hydroxy-sn-glycero-3-phosphocholine	16:0-Lyso PC
Diacylglycerol	DAG	N/A	N/A

1027

1028 **Figure Legends:**

1029
1030
1031 Figure 1: Membrane Remodeling in M. Mycoides is Dependent on Acyl Chain Scavenging
1032
1033 1 *Mycoplasma mycoides* can take up phospholipids and free fatty acids from its environment. 2
1034 Cleaving ester bonds from glycerophospholipids results in a pool of free fatty acids. 3 With fatty
1035 acids, *M. mycoides* is able to synthesize Phosphatidylglycerol (PG) with various fatty acid
1036 compositions, as well as remodel other phospholipid classes. 4 Cardiolipin (CL) can be synthesized
1037 from two PGs, starting with cleavage of PG headgroups. 5 *M. mycoides* can synthesize a variety
1038 of Cardiolipins from PG. 6 Cleaving acyl chains from remodeled and synthesized phospholipids
1039 replenishes the pool of free fatty acids. 7 Glycerophospholipids are inserted into the membrane.
1040 8 Cholesterol is essential for *M. Mycoides* growth.
1041
1042
1043 Figure 2: A Defined Lipid Diet Results in a Living Membrane with Two Lipids
1044
1045 a *M. mycoides* can adapt to defined lipid "diets" with diester or diether phospholipids; resulting
1046 in simpler membranes than when grown on a complex diet (e.g. FBS). Adaptation to new diets
1047 occurs after 3 passages ($p > 3$). TLC aspect ratio adjusted for legibility; unmodified TLCs can be
1048 found in Figure S2. *M. mycoides* can scavenge acyl chains from POPC, yielding a more complex
1049 membrane from a defined diet. b Lipidomic analysis of cells grown on only oleic and palmitic acid
1050 shows *M. mycoides* cells can synthesize Phosphatidylglycerol and Cardiolipin species when a
1051 source of fatty acids is present. c Lipidomic analysis of *M. mycoides* cells grown on a POPC +
1052 Cholesterol diet shows acyl chain scavenging leads to the synthesis of a diversity of lipids,
1053 resulting in a membrane with 28 lipids from a diet of only two. d 16:0-18:1 diether PC has ether-
1054 linked hydrocarbon chains that cannot be cleaved by *M. mycoides*, eliminating scavenging.
1055 Lipidomic analysis shows living cells with two lipids comprising 99.9 mol% of their lipidome.
1056
1057
1058 Figure 3: Living Membranes with Tunable Lipid Class and Acyl Chain Complexity
1059
1060 a 16:0-18:1 Diether PG diet results in the synthesis of Cardiolipin with fully ether-linked
1061 hydrocarbon chains, increasing head group, but not acyl chain complexity. b A diet of both
1062 Diether PC and PG restores the headgroup, but not acyl chain, complexity of the POPC diet. c
1063 When switched from one diet to another, in this case from the D.PC diet to the POPC diet, there
1064 is an adaptation period before acyl chain scavenging occurs. d A diet derived from a total lipid
1065 extract of cells grown on the POPC diet (a "transplant" diet) restores the full complexity of the

1066 POPC. Growth on this transplanted diet was performed after the first passage (p = 1) to the new
1067 diet, before cells begin to scavenge acyl chains from exogenous phospholipids. e Reintroducing
1068 acyl chain complexity is more effective than headgroup complexity for rescuing growth (relative
1069 to cells adapted to a POPC diet), but, even when full complexity is restored, acyl chain scavenging
1070 capacity still improves growth. P-values, calculated using a two-tailed Student's-t-test, are shown
1071 when relevant. N, number of replicates, for all growth rates can be found in table S1.
1072
1073 Figure 4: Lipidome Minimization in JCVI-Syn3A: Achieving a Minimal Membrane in a Genomically
1074 Minimal Cell
1075
1076 a JCVI-Syn3A exhibits growth rates similar to *M. mycoides* on a minimal lipid diet. b JCVI-Syn3A is
1077 viable when grown on a Diether-PC + Cholesterol diet with 99.34 mol% of the membrane
1078 comprised of only two lipids. c JCVI-Syn3A cells display three phenotypes when observed with
1079 Transmission Electron Microscopy; a normal ovoid morphology, cells with internal membranes,
1080 and cells with intercellular tubules. Cell counts reveal the Diether-PC diet yields significantly more
1081 cells with the internal membranes than the other diets. Cell counts can be found in Figure S6a-
1082 S6g d A tomogram of a JCVI-Syn3A cell on the Diether-PC diet with internal membranes reveals
1083 a large cell with multiple membrane-bound internal vesicle-like structures that have a lower
1084 electron density compared to the rest of the cell, suggesting the internal membrane bound
1085 structures are vesicles occurring from membrane invagination. Modeling shows these vesicles
1086 are completely enclosed and separate from the cell surface membrane. Images in this figure are
1087 from a single biological replicate. P-values, calculated using a two-tailed Student's-t-test, are
1088 shown when relevant. N, number of replicates for all growth rates, can be found in table S1.
1089
1090
1091 Figure 5: Enantiomeric Lipid Diets Negatively Affect Cell Growth and Membrane Properties
1092
1093 a Enantiomeric (Ent) POPC is a synthetic chiral POPC with the head group in the SN1 position,
1094 rather than SN3 position. b *M. mycoides* and c JCVI-Syn3A cells exhibit slower growth when grown
1095 on diets with enantiomeric POPC present; are more fragile to hypoosmotic shock when grown on
1096 diets with enantiomeric POPC present; and are more permeable to non-chiral fluorescein
1097 diacetate (FDA) when grown on diets with enantiomeric POPC present. d M. mycoides and e JCVI-
1098 Syn3A cell growth and membrane permeability are inversely correlated. P-values, calculated
1099 using a two-tailed Student's-t-test, are shown when relevant. N, number of replicates for all
1100 growth rates, can be found in table S1. N=3 biological replicates for osmotic sensitivity and
1101 permeability subfigures.
1102
1103

1104

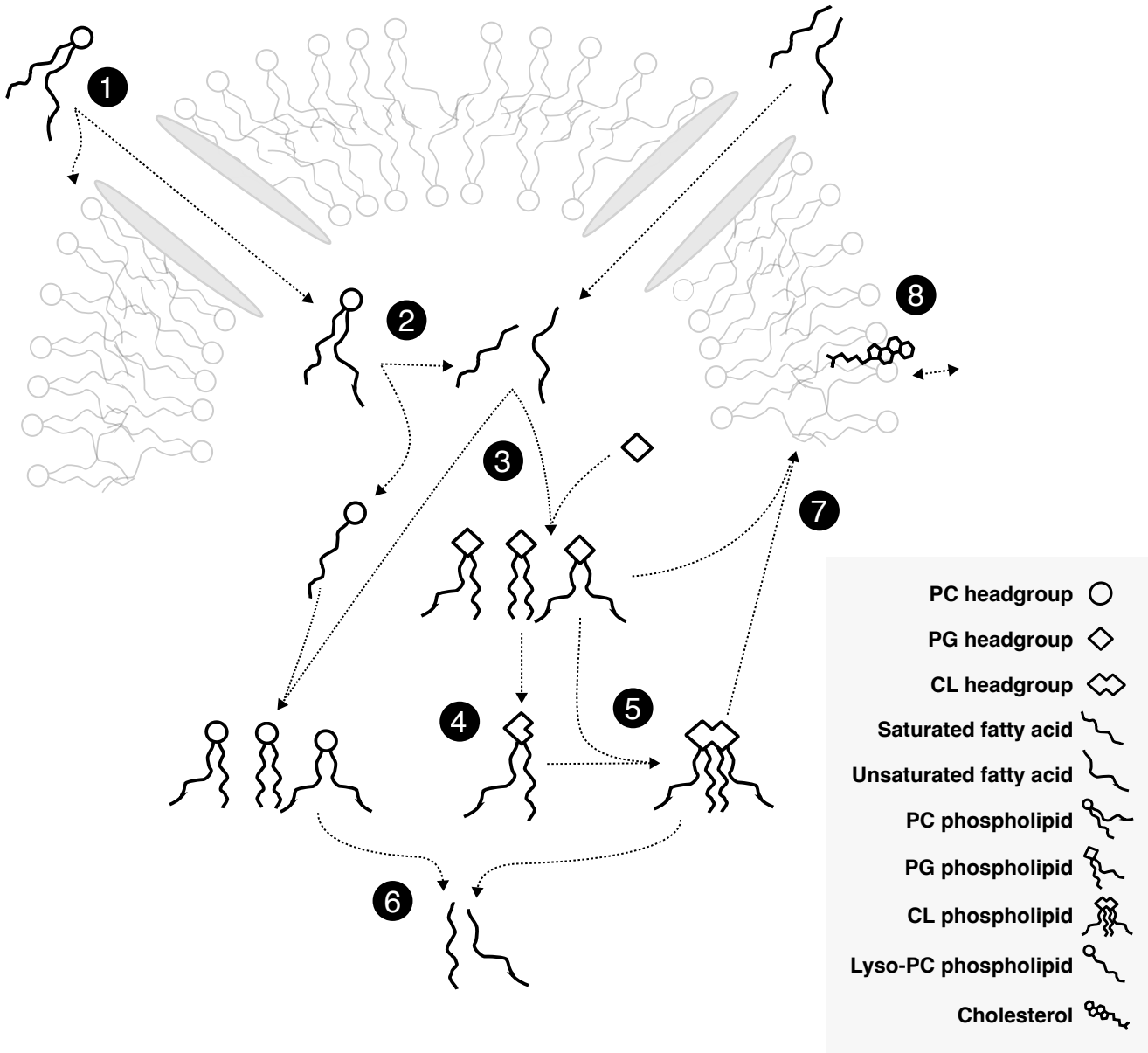

Figure 1: Membrane Remodeling in *M. Mycoides* is Dependent on Acyl Chain Scavenging

1 *Mycoplasma mycoides* can take up phospholipids and free fatty acids from its environment. **2** Cleaving ester bonds from glycerophospholipids results in a pool of free fatty acids. **3** With fatty acids, *M. mycoides* is able to synthesize Phosphatidylglycerol (PG) with various fatty acid compositions, as well as remodel other phospholipid classes. **4** Cardiolipin (CL) can be synthesized from two PGs, starting with cleavage of PG headgroups. **5** *M. mycoides* can synthesize a variety of Cardiolipins from PG. **6** Cleaving acyl chains from remodeled and synthesized phospholipids replenishes the pool of free fatty acids. **7** Glycerophospholipids are inserted into the membrane. **8** Cholesterol is essential for *M. Mycoides* growth.

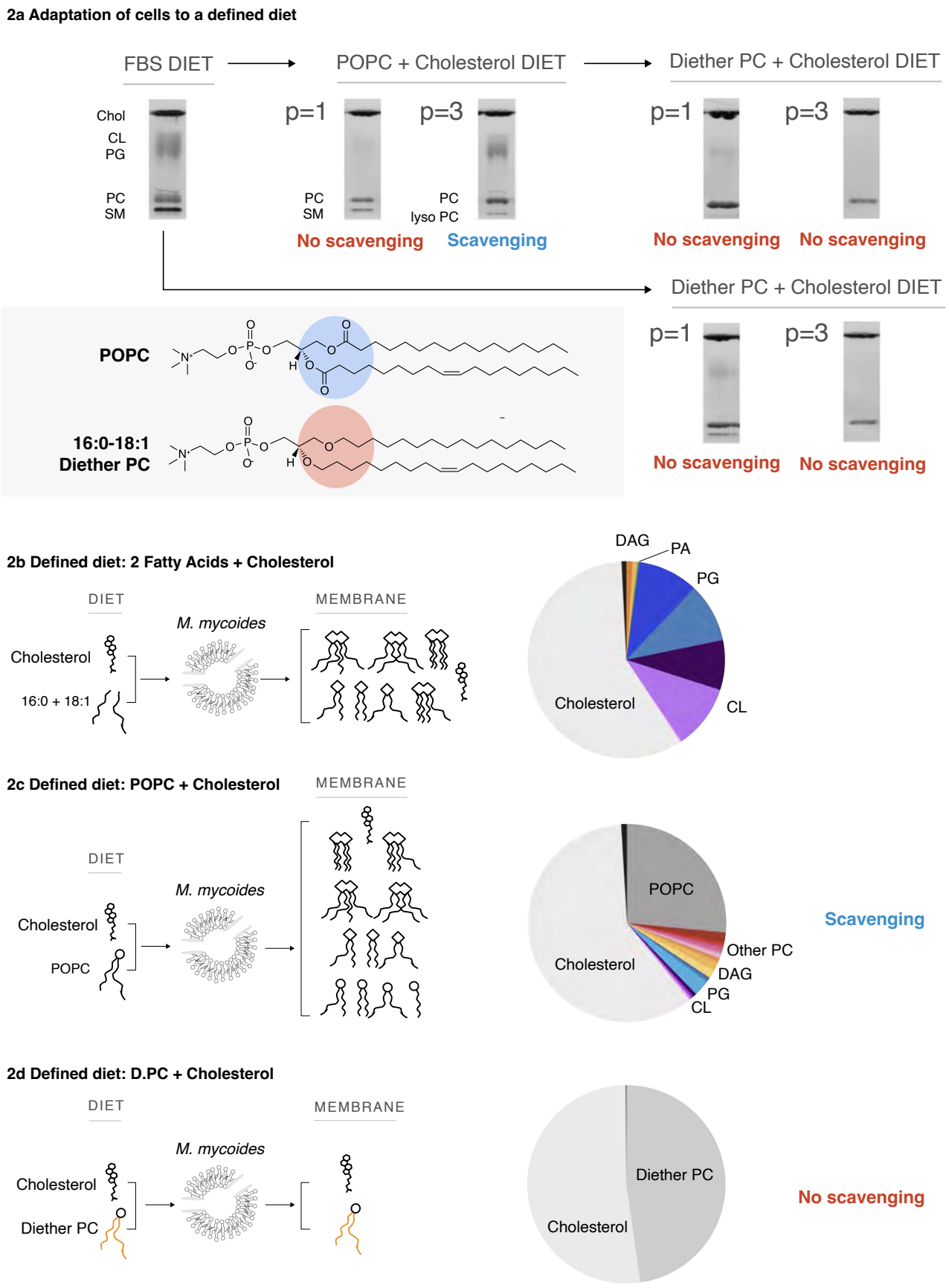

Figure 2: A Defined Lipid Diet Results in a Living Membrane with Two Lipids

a *M. mycoides* can adapt to defined lipid "diets" with diester or diether phospholipids; resulting in simpler membranes than when grown on a complex diet (e.g. FBS). Adaptation to new diets occurs after 3 passages ($p > 3$). TLC aspect ratio adjusted for legibility; unmodified TLCs can be found in Figure S2. *M. mycoides* can scavenge acyl chains from POPC, yielding a more complex membrane from a defined diet. **b** Lipidomic analysis of cells grown on only oleic and palmitic acid shows *M. mycoides* cells can synthesize Phosphatidylglycerol and Cardiolipin species when a source of fatty acids is present. **c** Lipidomic analysis of *M. mycoides* cells grown on a POPC + Cholesterol diet shows acyl chain scavenging leads to the synthesis of a diversity of lipids, resulting in a membrane with 28 lipids from a diet of only two. **d** 16:0-18:1 diether PC has ether-linked hydrocarbon chains that cannot be cleaved by *M. mycoides*, eliminating scavenging. Lipidomic analysis shows living cells with two lipids comprising 99.9 mol% of their lipidome.

3a Defined diet: D.PG + Cholesterol

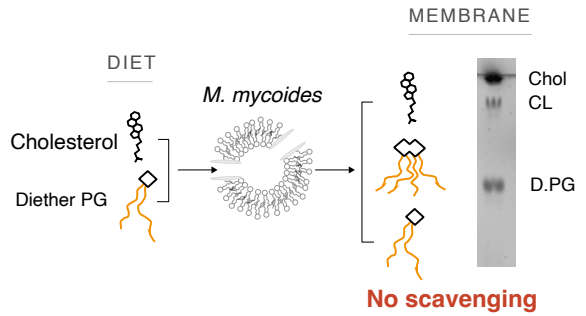

3b Defined diet: D.PC + D.PG + Cholesterol

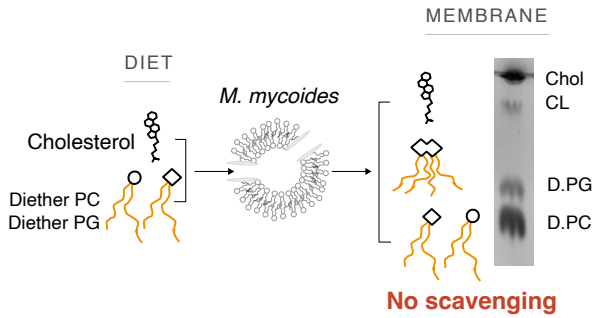

3c Defined diet: POPC + Cholesterol diet after first passage

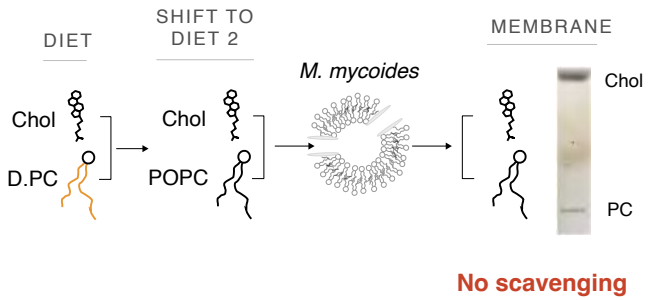

3d Defined diet: Membrane Transplant

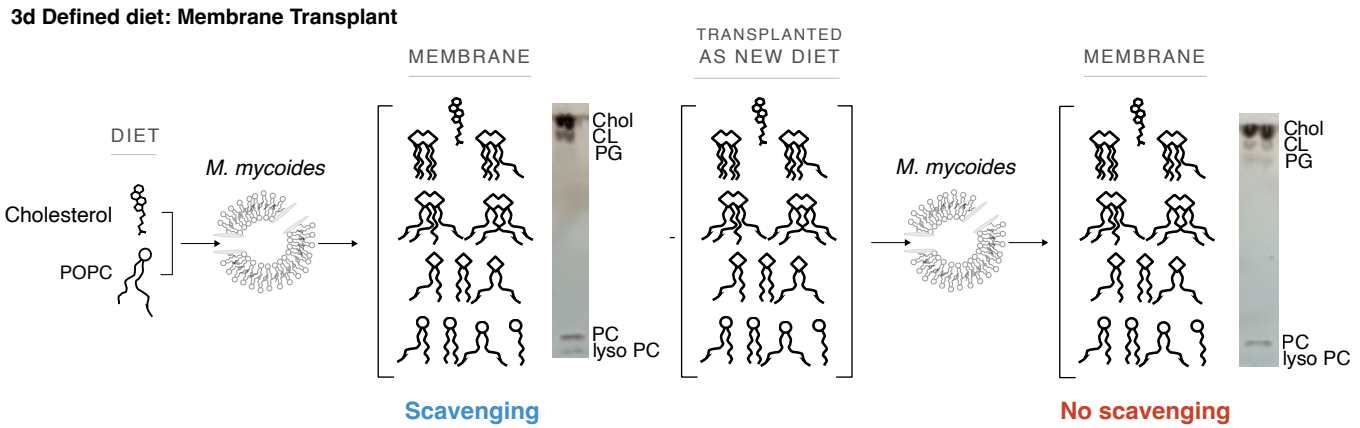

3e *M. mycoides* Growth Rates on Defined Diets

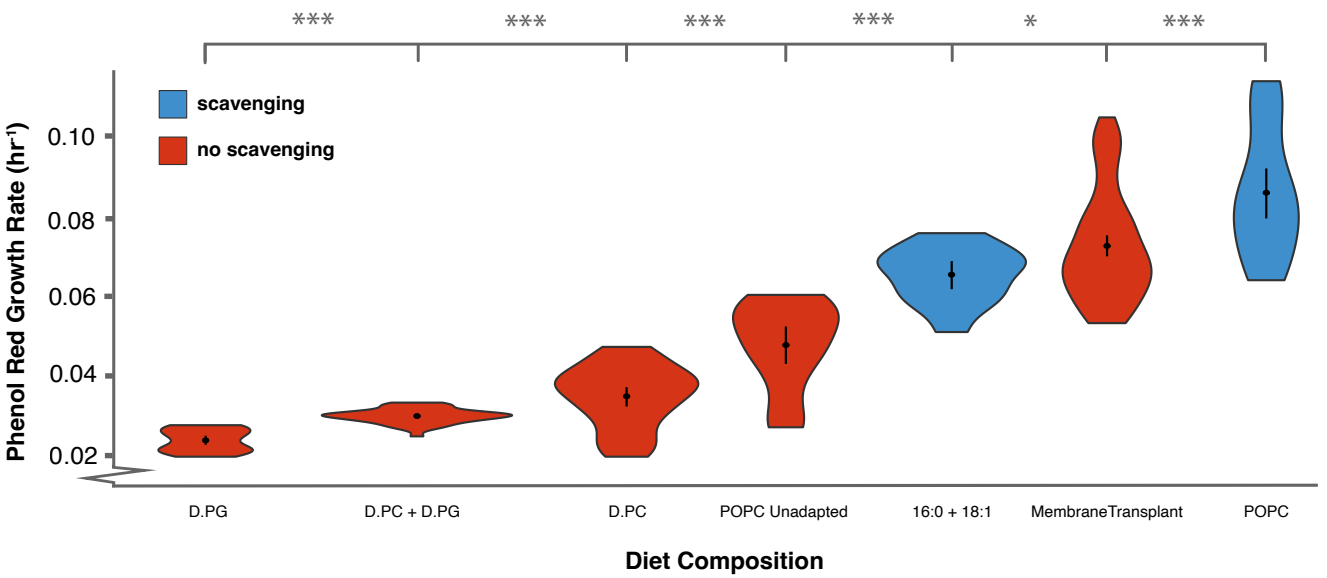

Figure 3: Living Membranes with Tunable Lipid Class and Acyl Chain Complexity

a 16:0-18:1 Diether PG diet results in the synthesis of Cardiolipin with fully ether-linked hydrocarbon chains, increasing head group, but not acyl chain complexity. **b** A diet of both Diether PC and PG restores the headgroup, but not acyl chain, complexity of the POPC diet. **c** When switched from one diet to another, in this case from the D.PC diet to the POPC diet, there is an adaptation period before acyl chain scavenging occurs. **d** A diet derived from a total lipid extract of cells grown on the POPC diet (a "transplant" diet) restores the full complexity of the POPC. Growth on this transplanted diet was performed after the first passage (p = 1) to the new diet, before cells begin to scavenge acyl chains from exogenous phospholipids. **e** Reintroducing acyl chain complexity is more effective than headgroup complexity for rescuing growth (relative to cells adapted to a POPC diet), but, even when full complexity is restored, acyl chain scavenging capacity still improves growth. Error bars are mean +/- SD. * equals p-value < 0.1; ** equals p-value < 0.05; *** equals p-value < 0.01. N, number of replicates, for all growth rates was 5 or greater and can be found in Supplementary Table S2.

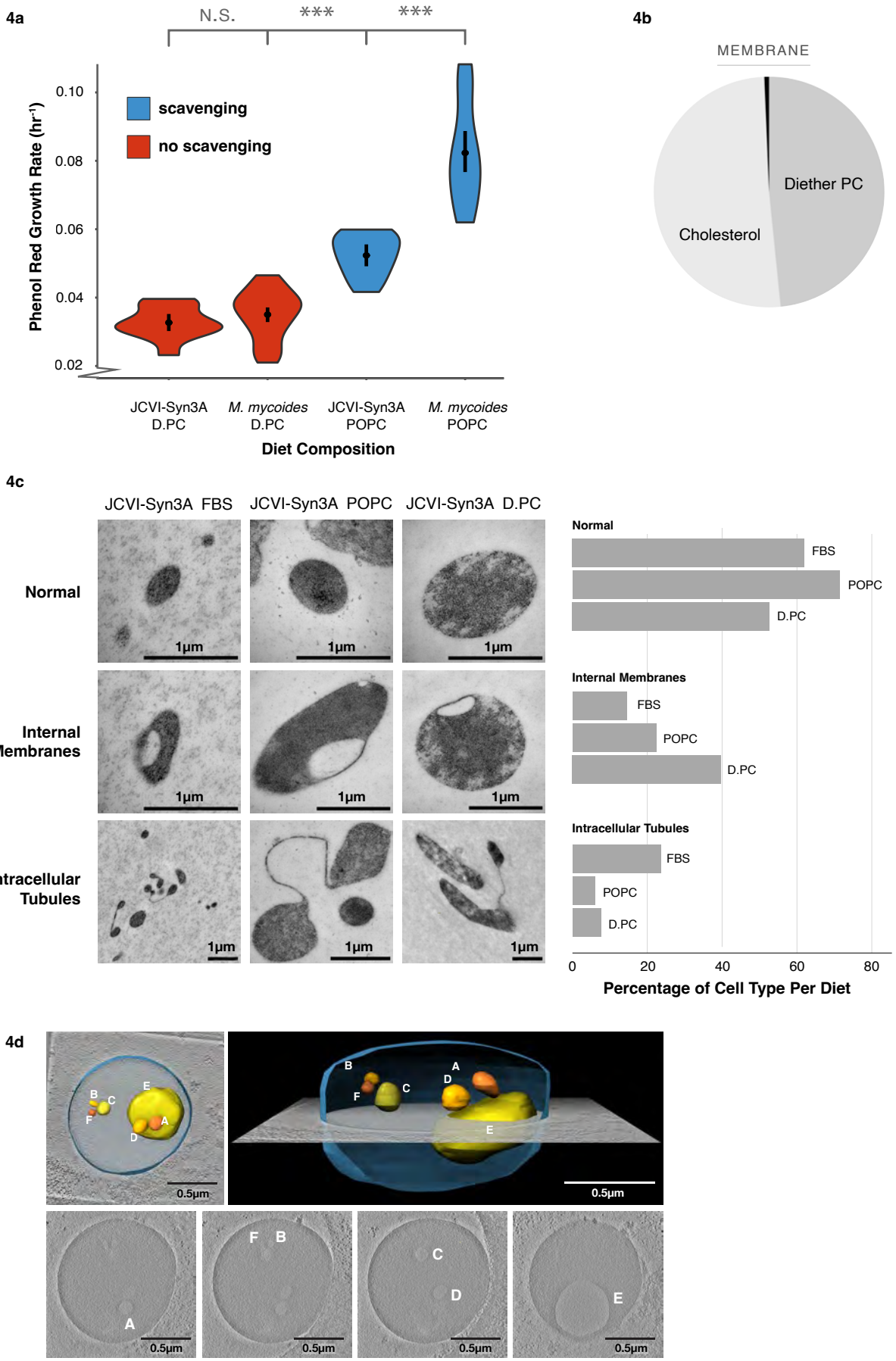

Figure 4: Lipidome Minimization in JCVI-Syn3A: Achieving a Minimal Membrane in a Genomically Minimal Cell

a JCVI-Syn3A exhibits growth rates similar to *M. mycoides* on a minimal lipid diet. **b** JCVI-Syn3A is viable when grown on a Diether-PC + Cholesterol diet with 99.34 mol% of the membrane comprised of only two lipids. **c** JCVI-Syn-3A cells display three phenotypes when observed with Transmission Electron Microscopy; a normal ovoid morphology, cells with internal membranes, and cells with intracellular tubules. Cell counts reveal the Diether-PC diet yields significantly more cells with the internal membranes than the other diets. Cell counts can be found in Figure S6a-S6g **d** A tomogram of a JCVI-Syn3A cell on the Diether-PC diet with internal membranes reveals a large cell with multiple membrane-bound internal vesicle-like structures that have a lower electron density compared to the rest of the cell, suggesting the internal membrane bound structures are vesicles occurring from membrane invagination. Modeling shows these vesicles are completely enclosed and separate from the cell surface membrane. Error bars are mean +/- SD. * equals p-value < 0.1; ** equals p-value < 0.05; *** equals p-value < 0.01. N, number of replicates for all growth rates, was 5 or greater and can be found in Supplementary Table S2.

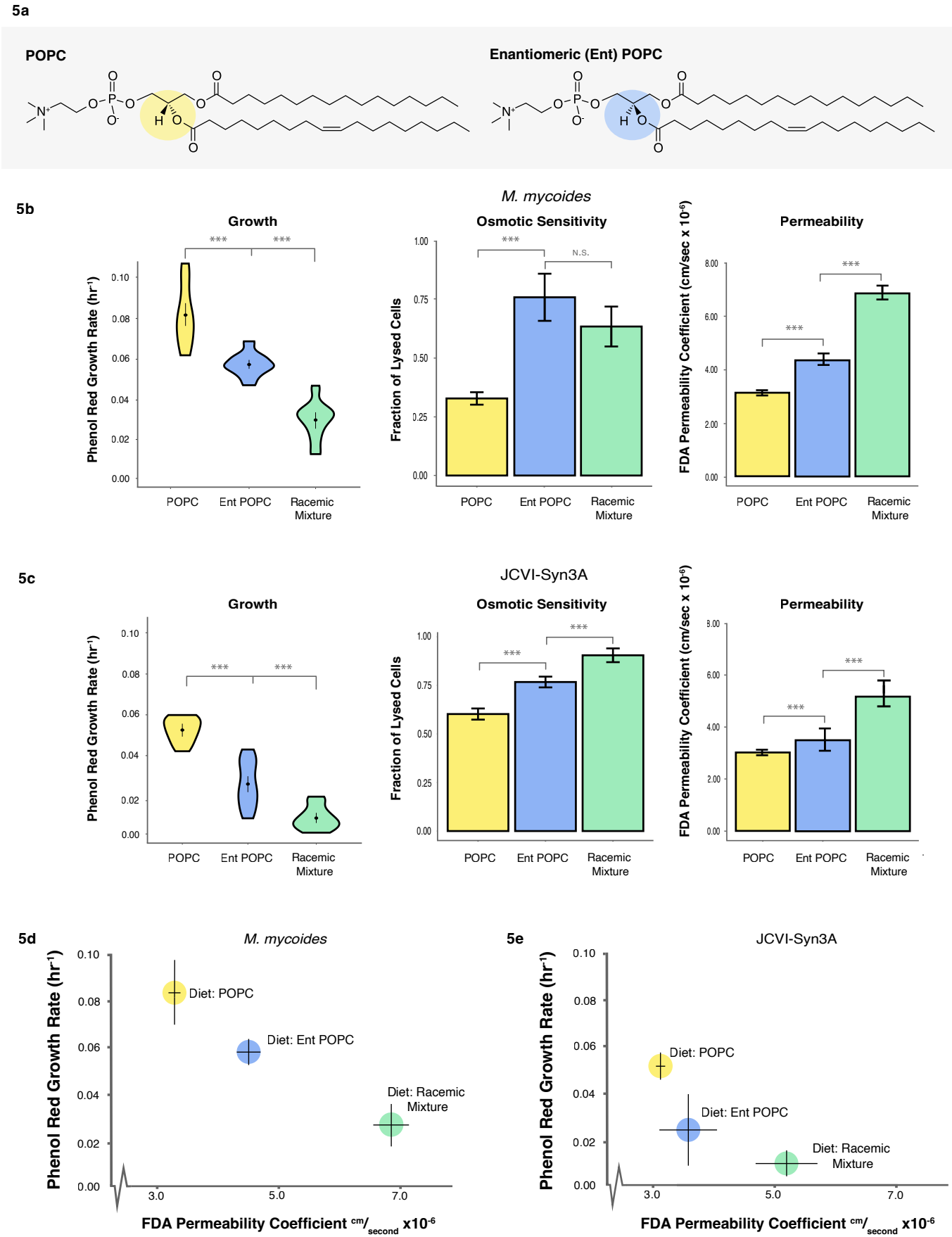

Figure 5: Enantiomeric Lipid Diets Negatively Affect Cell Growth and Membrane Properties

a Enantiomeric (Ent) POPC is a synthetic chiral POPC with the head group in the SN1 position, rather than SN3 position. **b** *M. mycoides* and **c** JCVI-Syn3A cells exhibit slower growth when grown on diets with enantiomeric POPC present; are more fragile to hypoosmotic shock when grown on diets with enantiomeric POPC present; and are more permeable to non-chiral fluorescein diacetate (FDA) when grown on diets with enantiomeric POPC present. **d** *M. mycoides* and **e** JCVI-Syn3A cell growth and membrane permeability are inversely correlated. Error bars are mean +/- SD. * equals p-value < 0.1; ** equals p-value < 0.05; *** equals p-value < 0.01. N, number of replicates, for all growth rates was 5 or greater and can be found in Supplementary Table S2. N=3 for osmotic sensitivity and permeability subfigures.

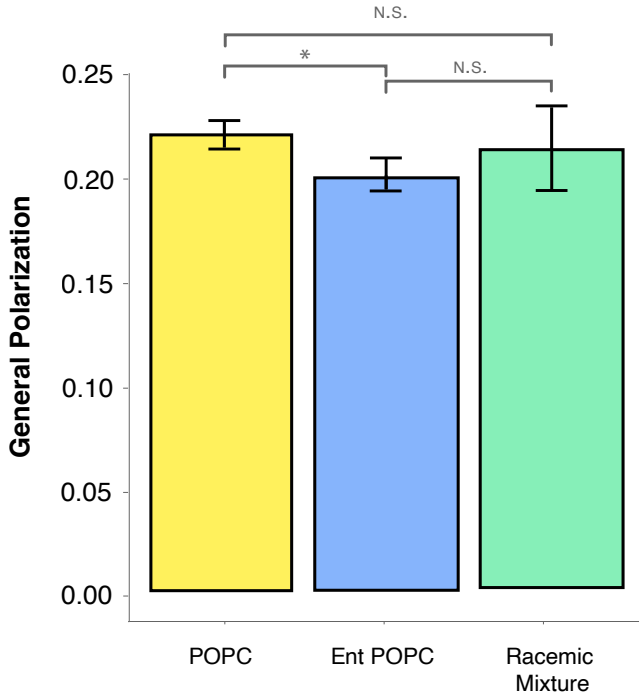

Figure 6: Enantiomeric Lipids Have no Significant Effect on Lipid Order

Lipid vesicles reconstituted from total lipid extracts of *M. mycoides* cells had a similar lipid order (measured as the general polarization index of c-laurdan) for all three diets with POPC enantiomers. Error bars are mean +/- SD. * equals p-value < 0.1; ** equals p-value < 0.05; *** equals p-value < 0.01. N=3